responders at 6 weeks (9 of 12 patients in the DAL-HX study, 24 of 29 patients in the LCH-1 study, and 2 of 3 patients in the current JLSG-96 study). Increasing the response rate at the induction of treatment and the prompt rescue of poor responders to initial therapy are imperative to improve therapeutic results for pediatric patients with multifocal LCH. We applied our Arm B protocol—a salvage regimen—for such poor responders. This rescue protocol resulted in the survival of 12 of 14 poor responders (85.7%) in our JLSG-96 study. In contrast, 30.8% and 64.2% of poor responders survived in the DAL-HX and LCH-I studies, respectively. Thus, our very low mortality rates appear to result at least in part from the high response rates to the Induction Arm A regimen and the high rescue rates with the Arm B regimen.

Some aspects of our the current results were unsatisfactory, namely, the low EFS rate (<40%) and the high reactivation rate (45.3%) in the MS group. To improve the quality of life for pediatric patients with LCH, we have modified our treatment protocol. Our ongoing protocol (JLSG-02) has been revised as follows; first, we have increased the initial dosage of PSL (2 mg/kg per day continuously for 4 weeks) from that in the JLSG-96 protocol (2 mg/kg per day for 5 days every 2 weeks); second, we added cyclosporine A to the Arm B Induction regimen for patients with PD; and third, we extended the treatment duration from 7.5 months to 1 year. Because rescuing patients with PD who have MS-type LCH is crucial for improving their survival rate, experimental trials that include more aggressive therapy, such as combination chemotherapy with 2-chlorodeoxyadenosine and high-dose Ara-C[18] or hematopoietic stem cell transplantation with myeloablative or reduced intensity conditionings,[19,20] must be carried out carefully. These therapies should be incorporated into future protocols for patients with refractory and progressive LCH in well designed, large-scale clinical studies.

REFERENCES

1. Laman JD, Leenen PJ, Annels NE, Hogendoorn PC, Egeler RM. Langerhans-cell histiocytosis 'insight into DC biology.' *Trends Immunol.* 2003;24:190–196.
2. Imashuku S, Ikushima S, Hibi S, Todo S. Langerhans cell histiocytosis and hemophagocytic syndrome in Japan; epidemiological studies. *Int J Pediatr Hematol Oncol.* 1994;1: 241–246.
3. Gadner H, Ladisch S. The treatment of Langerhans cell histiocytosis. In: Weitzman S, Egeler RM, editors. *Histiocytic Disorders of Children and Adults; Basic Science, Clinical Features and Therapy.* Cambridge: Cambridge University Press; 2005: 229–253.
4. Donadieu J, Egeler RM, Pritchard J. Langerhans cell histiocytosis: a clinical update. In: Weitzman S, Egeler RM, editors. *Histiocytic Disorders of Children and Adults; Basic Science, Clinical Features and Therapy.* Cambridge: Cambridge University Press; 2005:95–129.
5. Lahey ME. Histiocytosis X—comparison of three treatment regimens. *J Pediatr.* 1975;87:179–183.
6. Ceci A, de Terlizzi M, Colella R, et al. Langerhans cell histiocytosis in childhood: results from the Italian Cooperative AIEOP-CNR-H.X '83 study. *Med Pediatr Oncol.* 1993;21: 259–264.
7. Gadner H, Heitger A, Grois N, Gatterer-Menz I, Ladisch S. Treatment strategy for disseminated Langerhans cell histiocytosis. DAL HX-83 Study Group. *Med Pediatr Oncol.* 1994;23: 72–80.
8. Minkov M, Grois N, Heitger A, Potschger U, Westermeier T, Gadner H. Treatment of multisystem Langerhans cell histiocytosis. Results of the DAL-HX 83 and DAL-HX 90 studies. DAL-HX Study Group. *Klin Padiatr.* 2000;212:139–144.
9. Gadner H, Grois N, Arico M, et al., Histiocyte Society. A randomized trial of treatment for multisystem Langerhans' cell histiocytosis. *J Pediatr.* 2001;138:728–734.
10. Haupt R, Nanduri V, Calevo MG, et al. Permanent consequences in Langerhans cell histiocytosis patients: a pilot study from the Histiocyte Society-Late Effects Study Group. *Pediatr Blood Cancer.* 2004;42:438–444.
11. Grois N, Prayer D, Prosch H, Lassmann H, CNS LCH Cooperative Group. Neuropathology of CNS disease in Langerhans cell histiocytosis. *Brain.* 2005;128(Pt 4):829–838.
12. Egeler RM, Neglia JP, Arico M, et al. The relation of Langerhans cell histiocytosis to acute leukemia, lymphomas, and other solid tumors. The LCH-Malignancy Study Group of the Histiocyte Society. *Hematol Oncol Clin North Am.* 1998;12: 369–378.
13. Lahey E. Histiocytosis X—an analysis of prognostic factors. *J Pediatr.* 1975;87:184–189.
14. Imashuku S, Ishida S, Koike K, et al., Japan LCH Study Group. Cerebellar ataxia in pediatric patients with Langerhans cell histiocytosis. *J Pediatr Hematol Oncol.* 2004;26:735–739.
15. Titgemeyer C, Grois N, Minkov M, Flucher-Wolfram B, Gatterer-Menz I, Gadner H. Pattern and course of single-system disease in Langerhans cell histiocytosis data from the DAL-HX 83- and 90-study. *Med Pediatr Oncol.* 2001;37: 108–114.
16. Egeler RM, de Kraker J, Voute PA. Cytosine-arabinoside, vincristine, and prednisolone in the treatment of children with disseminated Langerhans cell histiocytosis with organ dysfunction: experience at a single institution. *Med Pediatr Oncol.* 1993;21:265–270.
17. Minkov M, Grois N, Heitger A, Potschger U, Westermeier T, Gadner H, DAL-HX Study Group. Response to initial treatment of multisystem Langerhans cell histiocytosis: an important prognostic indicator. *Med Pediatr Oncol.* 2002;39:581–585.
18. Bernard F, Thomas C, Bertrand Y, et al. Multi-centre pilot study of 2-chlorodeoxyadenosine and cytosine arabinoside combined chemotherapy in refractory Langerhans cell histiocytosis with haematological dysfunction. *Eur J Cancer.* 2005;41:2682–2689.
19. Suminoe A, Matsuzaki A, Hattori H, Ishii S, Hara T. Unrelated cord blood transplantation for an infant with chemotherapy-resistant progressive Langerhans cell histiocytosis. *J Pediatr Hematol Oncol.* 2001;23:633–636.
20. Steiner M, Matthes-Martin S, Attarbaschi A, et al. Improved outcome of treatment-resistant high-risk Langerhans cell histiocytosis after allogeneic stem cell transplantation with reduced-intensity conditioning. *Bone Marrow Transplant.* 2005;36: 215–225.

High Serum Values of Soluble CD154, IL-2 Receptor, RANKL and Osteoprotegerin in Langerhans Cell Histiocytosis

Rumiko Ishii, MD,[1]* Akira Morimoto, MD,[1] Satoshi Ikushima, MD,[2] Tohru Sugimoto, MD,[1] Keiko Asami, MD,[3] Fumio Bessho, MD,[4] Kazuko Kudo, MD,[5] Yukiko Tsunematu, MD,[6] Junichiro Fujimoto, MD,[7] and Shinsaku Imashuku, MD[8]

Background. To determine useful biochemical markers in Langerhans cell histiocytosis (LCH), we analyzed the serum levels of soluble CD154 (sCD154), IL2 receptor (sIL2-R), receptor activator of NF-κB ligand (sRANKL), and osteoprotegerin (OPG). *Procedure.* Our study included 46 newly diagnosed LCH patients (single-system multi-site (SM type): $n=20$, and multi-system multi-site (MM type): $n=26$) who were treated with the JLSG-02 protocol between 2002 and 2004. The median age of the patients was 3.8 years old (range 0–18). sCD154, sIL2-R, sRANKL, and OPG were measured by ELISA at diagnosis ($n=46$) and after 6-weeks of induction therapy ($n=14$). *Results.* The values of sCD154, sIL-2R, sRANKL, and OPG, and the sRANKL/OPG ratio in sera were significantly higher in patients with LCH compared with controls (1.83 ± 1.38 vs. 0.22 ± 0.16 ng/ml, $P<0.001$; $1,600\pm1,060$ vs. 420 ± 160 pg/ml, $P<0.001$; 1.72 ± 1.20 vs. 1.04 ± 1.09 pmol/L, $P=0.019$; 6.34 ± 2.94 vs. 3.71 ± 2.03 pmol/L, $P<0.001$; and 0.40 ± 0.45 vs. 0.16 ± 0.17, $P=0.023$, respectively). Serum levels of sIL-2R were significantly elevated in the MM type compared with the SM type ($2,050\pm1,060$ vs. 870 ± 340 pg/ml, $P<0.001$). Serum OPG levels were also significantly elevated in the MM type compared with the SM type (7.58 ± 2.72 vs. 5.13 ± 2.69 pmol/L, $P=0.008$) and negatively correlated with the number of bone lesions ($r=-0.56$, $P=0.007$). In contrast, the sRANKL/OPG ratios were significantly higher in the SM type than the MM type (0.57 ± 0.54 vs. 0.19 ± 0.14, $P=0.002$) and positively correlated with the number of bone lesions ($r=0.34$, $P=0.040$). In patients who responded to the induction therapy, serum levels of sIL-2R, sRANKL, and OPG, and the sRANKL/OPG ratio decreased significantly after the therapy ($1,170\pm600$ vs. 730 ± 290 pg/ml, $P=0.029$; 2.19 ± 1.06 vs. 1.24 ± 0.66 pmol/L, $P<0.001$; 6.13 ± 2.40 vs. 4.72 ± 2.03 pmol/L, $P=0.040$; and 0.57 ± 0.52 vs. 0.41 ± 0.37, $P=0.02$, respectively). In the three patients who did not respond to the induction therapy, the serum levels of sCD154 increased significantly after the therapy (1.3 ± 1.1 vs. 2.7 ± 1.2, $P=0.004$). *Conclusions.* Serum levels of sIL-2R and sCD154 could be useful as indicators of inflammation and sRANKL/OPG ratios as markers of osteolytic activity in LCH patients. Pediatr Blood Cancer © 2005 Wiley-Liss, Inc.

Key words: CD154; IL2 receptor; Langerhans cell histiocytosis; osteoprotegerin; receptor activator of NF-κB

INTRODUCTION

Langerhans cell histiocytosis (LCH) is a rare clonal disease involving the bone, skin, soft tissue, and other organs. The clinical features of LCH vary from a self-healing single system lesion to chemotherapy-resistant fatal multi-system involvement and organ dysfunction. Although the precise pathogenesis of LCH is obscure, cytokines are thought to be involved in both the localized tissue disease as well as the systemic pathology of the disease [1].

Recently, Rosso et al. [2] reported that soluble IL-2 receptor (sIL-2R), interleukin-1 receptor antagonist (IL-1Ra) and tumor necrosis factor-alpha (TNF-alpha) [3] were useful clinical biological markers of LCH. In LCH lesions, many diverse cytokines are produced by pathological Langerhans cells and infiltrating T cells [4], and CD40 and CD40 ligand (designated as CD154) are expressed abundantly [5]. CD40, a member of the TNF receptor superfamily, is expressed mainly on B cells,

DOI 10.1002/pbc.20595

[1]Department of Pediatrics, Kyoto Prefectural University of Medicine, Graduate School of Medical Science, Kyoto, Japan

[2]Department of Pediatrics, Saiseikai Kyoto-fu Hospital, Kyoto, Japan

[3]Department of Pediatrics, Niigata Cancer Center Hospital, Niigata, Japan

[4]Department of Pediatrics, Kyorin University School of Medicine, Tokyo, Japan

[5]Department of Pediatrics, Nagoya University, Graduate School of Medicine, Nagoya, Japan

[6]Department of Strategic Medicine, Division of Pediatric Oncology, National Center for Child Health and Development, Tokyo, Japan

[7]Department of Developmental Biology and Pathology, National Research Institute for Child Health and Development, Tokyo, Japan

[8]Department of Pediatrics, Takasago-seibu Hospital, Takasago, Japan

*Correspondence to: Rumiko Ishii, Department of Pediatrics, Kyoto Prefectural University of Medicine, Graduate School of Medical Science, 465, Kajii-cho, Kawaramachi-Hirokoji, Kamigyo-ku, Kyoto 602-8566, Japan. E-mail: rumiko@koto.kpu-m.ac.jp

Received 8 March 2005; Accepted 22 July 2005

dendritic cells and macrophages. CD154 which also belongs to the TNF superfamily, is expressed on activated CD4-positive helper T cells and activated platelets, and easily becomes soluble in serum after activation. Interaction between CD40 and CD154 is known to play an important role in the activation, proliferation, and maturation of both T cells and antigen presenting cells (APCs) [6,7,8]. Soluble CD154 (sCD154) levels have been reported to be related to disease activities of systemic lupus erythematosus (SLE) [9] and rheumatoid arthritis (RA) [10], in association with an increased risk of cardiovascular events [11].

In osteolytic bone diseases, such as multiple myeloma, activation of osteoclasts plays an important osteolytic role in which the receptor activator of NF-κB (RANK), one of the cytokines related to TNF, is expressed on pre-osteoclasts. Pre-osteoclasts are differentiated into osteoclasts by the stimulation of RANK ligand (RANKL), which is expressed on osteoblasts and T cells. The RANKL binds to RANK as well as osteoprotegerin (OPG), which is secreted from osteoblasts and APCs to inhibit the binding of RANKL to RANK acting as a decoy receptor and regulate the formation of osteoclasts [12]. The soluble RANKL (sRANKL)/OPG ratio was previously reported to be a good clinical marker of malignant bone disease, such as multiple myeloma or bone metastases of breast cancer [13,14]. Therefore, such biological markers may be useful systemic monitors of LCH disease activity since bone lesions are one of the most prominent clinical features of LCH. We thus evaluated serum levels of sCD154, sIL-2R, sRANKL, and OPG in LCH patients. We found the levels are significantly higher in LCH patients and may be useful as biological markers of disease activity in LCH.

PATIENTS AND METHODS

Patients

Between April 2002 and September 2004, 46 newly diagnosed LCH patients with multiple lesions, all of whom were registered in the Japan LCH Study Group (JLSG)-02 protocol, were enrolled in this study. Informed consent was obtained from the parents in all cases. Twenty-eight were boys and 18 were girls. The median age of the patients was 3.8 years old (range 0–18). All patients diagnosed with histopathological findings of biopsied specimens were positive for at least s-100 or CD1a. We defined single-system multi-site (SM type) as multiple lesions in only one organ (n = 20), and multi-system multi-site (MM type) as multiple lesions in several organs (n = 26). Bone was the most commonly involved organ (n = 42), followed by skin (n = 15), lymph nodes (n = 7), liver/spleen (n = 7), pituitary (n = 3), and others (n = 10). All patients were treated with the 6-week induction therapy consisting of 2 mg/kg/day oral prednisolone (PSL) from day 1 to 28, 1 mg/kg/day from day 29 to 35, 0.5 mg/kg/day from day 36 to 42, vincristine (VCR) 0.05 mg/kg/day intravenous injection on day 1, 15, and 29, and cytarabine 100 mg/m^2/day 6-hr drip from day 1 to 5, day 15–19, and day 29–33. The maximum doses of PSL and VCR were 60 and 2 mg/day, respectively. After the 6-week induction therapy, patients considered to have a good response or a partial response (resolved more than 50% of lesions) were evaluated as responders, while patients with more than 50% of residual lesions and progressive disease were labeled as non-responders. At this point, 43 of the 46 patients responded to the induction chemotherapy and 45 patients were alive. One death from aggressive disease occurred at 8 weeks of therapy. Serum samples from 33 volunteer donors (median age 8.3 years, range 0–19) were used as normal controls.

Measurements of sCD154, sIL-2R, sRANKL, and OPG

Blood samples were obtained from the patients at the time of diagnosis (n = 46) and at the end of the 6-week induction therapy (n = 14, 11 responders and 3 non-responders). The samples were stored at −80 degrees until the time of analysis and not subjected to repeated freeze-thaw cycles. sCD154, sIL2-R, sRANKL, and OPG in each sample were measured in duplicate by the ELISA procedure using commercial kits according to the manufacturer's instructions (Bender Med Systems, Inc., BIO SOURCE, Inc., and BIOMEDICA Medizinprodukte GmbH and CoKG, Wien, respectively). In the assay, the standards were provided by the each commercial kit. The detection ranges of sCD154, sIL2-R, sRANKL, and OPG were; 0.095–10.0 ng/ml, 16–5,000 pg/ml, 0.08–8.0 pmol/L, and 0.14–30.0 pmol/L, respectively.

Statistical Analysis

Results are reported as mean ± standard deviation (SD). For the comparisons of the sCD154, sIL-2R, sRANKL, and OPG values, and sRANKL/OPG ratios, the Student's *t*-test was used between LCH patients and controls, between the SM type and the MM type, and between responders and non-responders, while two group paired *t*-test was used between before and after the induction therapy. The correlations among the serum levels of sCD154, sIL2R, sRANKL, and OPG, and sRANKL/OPG ratios, as well as correlations between the sRANKL and OPG values or sRANKL/OPG ratios and number of bone lesions, were assessed by the Spearman rank order test. A *P*-value of 0.05 or less was designated as statistically significant. All *P*-values were two-tailed.

RESULTS

Biological Marker Levels at Diagnosis

The serum levels of sCD154, sIL-2R sRANKL, and OPG, and sRANKL/OPG ratios were significantly higher

in patients with LCH compared with serum levels in controls (1.82 ± 1.39 vs. 0.22 ± 0.16 ng/ml, $P < 0.001$; $1,600 \pm 1,060$ vs. 420 ± 160 pg/ml, $P < 0.001$; 1.72 ± 1.20 vs. 1.04 ± 1.09 pmol/L, $P = 0.019$; 6.34 ± 2.94 vs. 3.71 ± 2.03 pmol/L, $P < 0.001$; and 0.40 ± 0.45 vs. 0.16 ± 0.17, $P = 0.017$, respectively) (Fig. 1). Serum levels of sCD154 and sRANKL did not differ significantly between the SM type and the MM type (Fig. 2A,C); however, serum levels of sIL-2R and OPG were significantly elevated in the MM type compared with the SM type ($2,050 \pm 1,070$ vs. 870 ± 340 pg/ml, $P < 0.001$ and 7.58 ± 2.72 vs. 5.13 ± 2.69 pmol/L, $P = 0.008$, respectively) (Fig. 2B,D). In contrast, sRANKL/OPG ratios were significantly higher in the SM type compared with the MM type (0.57 ± 0.54 vs. 0.19 ± 0.14, $P = 0.002$) (Fig. 2E). The number of bone lesions were negatively correlated with serum OPG levels and positively with sRANKL/OPG ratios ($n = 38$, $r = -0.56$, $P = 0.007$, and $r = 0.34$, $P = 0.040$, respectively) (Fig. 3A,B), but not with sRANKL levels (data not shown). On the other hand, there was no correlation between the value of sCD154, sIL2-R, sRANKL, and OPG and sRANKL/OPG ratios (data not shown).

Biological Marker Levels Before and After the 6-week Induction Therapy

We were able to obtain 14 pair samples before and after the 6-week induction therapy. In 11 responders, serum levels of sIL-2R, sRANKL, and OPG and sRANKL/OPG ratios significantly decreased after the therapy ($1,170 \pm 660$ vs. 730 ± 290 pg/ml, $P = 0.029$; 2.19 ± 1.06 vs. 1.24 ± 0.66 pmol/L, $P < 0.001$; 6.13 ± 2.40 vs. 4.72 ± 2.03 pmol/L, $P = 0.040$; and 0.57 ± 0.52 vs. 0.41 ± 0.37, $P = 0.021$, respectively) (Fig. 4a, B–E), while serum levels of sCD154 did not differ before and after the therapy (1.88 ± 1.52 vs. 1.15 ± 1.08 ng/ml, $P = 0.183$) (Fig. 4a, A). In three non-responders, the serum levels of sCD154 increased significantly after the therapy (1.30 ± 1.14 vs. 2.74 ± 1.17, $P = 0.004$) (Fig. 4b, A), while serum levels of sIL-2R, sRANKL, and OPG and sRANKL/OPG ratios did not differ before and after the therapy ($2,300 \pm 1,280$ vs. $1,700 \pm 1,020$ pg/ml, $P = 0.488$, 1.88 ± 1.20 vs. 2.53 ± 1.80 pmol/L, $P = 0.21$, 4.48 ± 1.13 vs. 4.39 ± 1.09 pmol/L, $P = 0.87$ and 0.29 ± 0.23 vs. 0.46 ± 0.32, $P = 0.120$) (Fig. 4b, B–E). The values of sCD154, sRANKL and OPG, and sRANKL/OPG ratios did not differ significantly between the responders and non-responders; however, serum levels of sIL2-R were significantly higher in the non-responders compared with the responders (data not shown).

DISCUSSION

We analyzed the serum levels of sCD154, sIL2-R, sRANKL, and OPG as well as sRANKL/OPG ratios to determine whether these biological markers are useful in the evaluation of LCH disease activity. All of these values were significantly higher in LCH patients compared with controls, indicating that they may reflect active LCH disease states, such as T cell and osteoclast activation in localized tumor tissues.

CD154 was previously revealed to be expressed on the surface of activated T cells as well as on activated platelets,

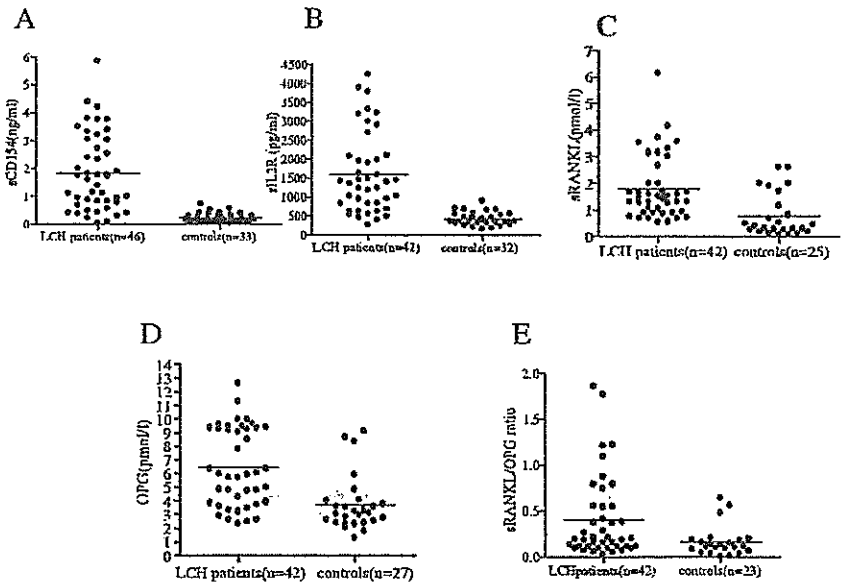

Fig. 1. Serum levels of sCD154, sIL-2R, sRANKL and OPG, and sRANKL/OPG ratios in LCH patients at diagnosis, compared with controls. A: sCD154; (B) sIL-2R; (C) sRANKL; (D) OPG; and (E) sRANKL/OPG ratios. Horizontal lines represent the mean value.

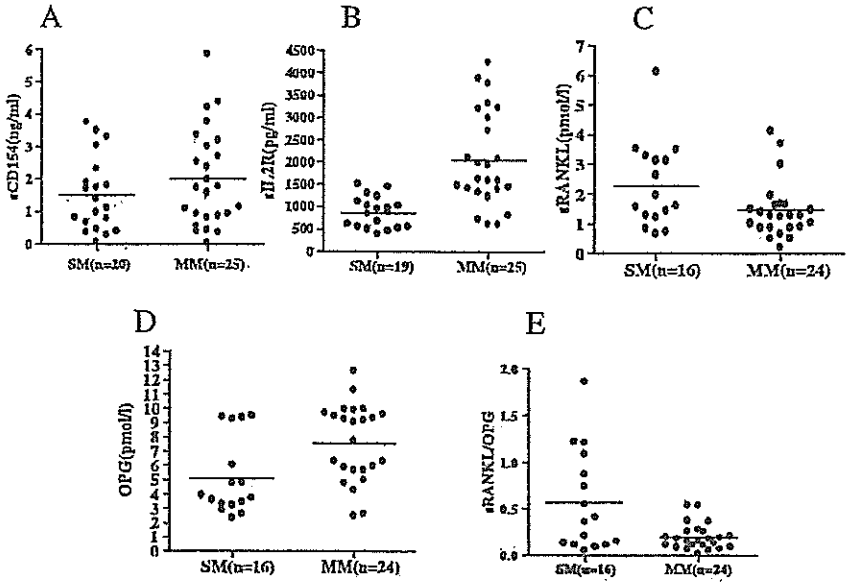

Fig. 2. Comparison of serum levels of sCD154, sIL2R, sRANKL and OPG, and sRANKL/OPG ratios between the SM and MM types at diagnosis. A: sCD154; (B) sIL-2R; and (C) sRANKL; (D) OPG; and (E) sRANKL/OPG ratios. Horizontal lines represent the mean value.

while CD40 is expressed on APCs as well as on B cells or endothelial cells. The CD40–CD154 interaction can occur not only between APCs and T cells, but also between B cells and T cells, and endothelial cells and platelets [6,7,8]. Upon T cell or platelet activation, CD154 is readily released into the serum; thus, sCD154 measurements may detect active immune states. Egeler et al. [5] found high expression levels of CD40 and CD154 in LCH tissues and assumed that these interactions play a key role in the pathogenesis of LCH. In this study, the sCD154 levels in LCH patients were significantly higher than levels in controls. However, the sCD154 levels in LCH patients were not as high as levels reported in SLE or RA patients [9,10]. In addition, sCD154 levels did not differ between the SM and the MM types, although serum levels steadily increased in non-responders. We assume that interactions between CD40 and CD154 in localized LCH lesions may be a limited reflection of systemic disease in patients, since several factors affect sCD154 levels due to the wide distribution of the CD40-CD154 system throughout the body.

Increased levels of sIL-2R, a truncated protein of the alpha chain of IL-2R expressed on T cells, have previously been reported in LCH [2,15]. Rosso et al. reported that sIL-2R levels correlated well with the disease stages of LCH (3,250 pg/ml in the single-system and 22,000 pg/ml in the multi-system types). Furthermore, patients with sIL-2R levels of greater than 17,500 pg/ml had significantly poor survival rates [2]. In this study, we also found that the sIL-2R levels were significantly higher in patients with the

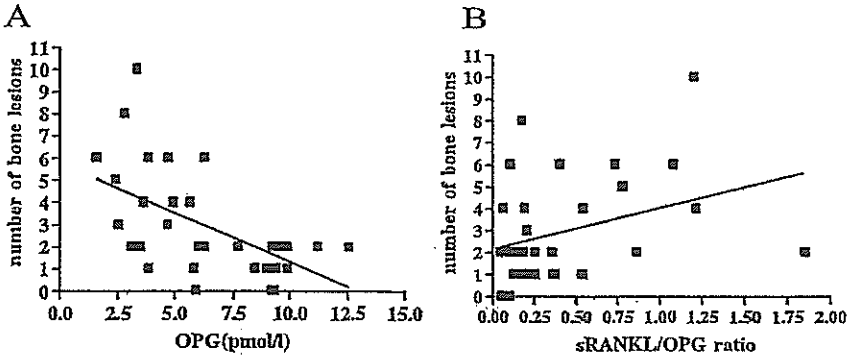

Fig. 3. Correlation between serum OPG levels (A) or sRANKL/OPG ratios (B) and number of involved bone lesions at diagnosis (n = 38). The number of bone lesions was negatively correlated with the serum OPG levels ($r = -0.56$, $P = 0.007$) and positively with sRANKL/OPG ($r = 0.34$, $P = 0.040$).

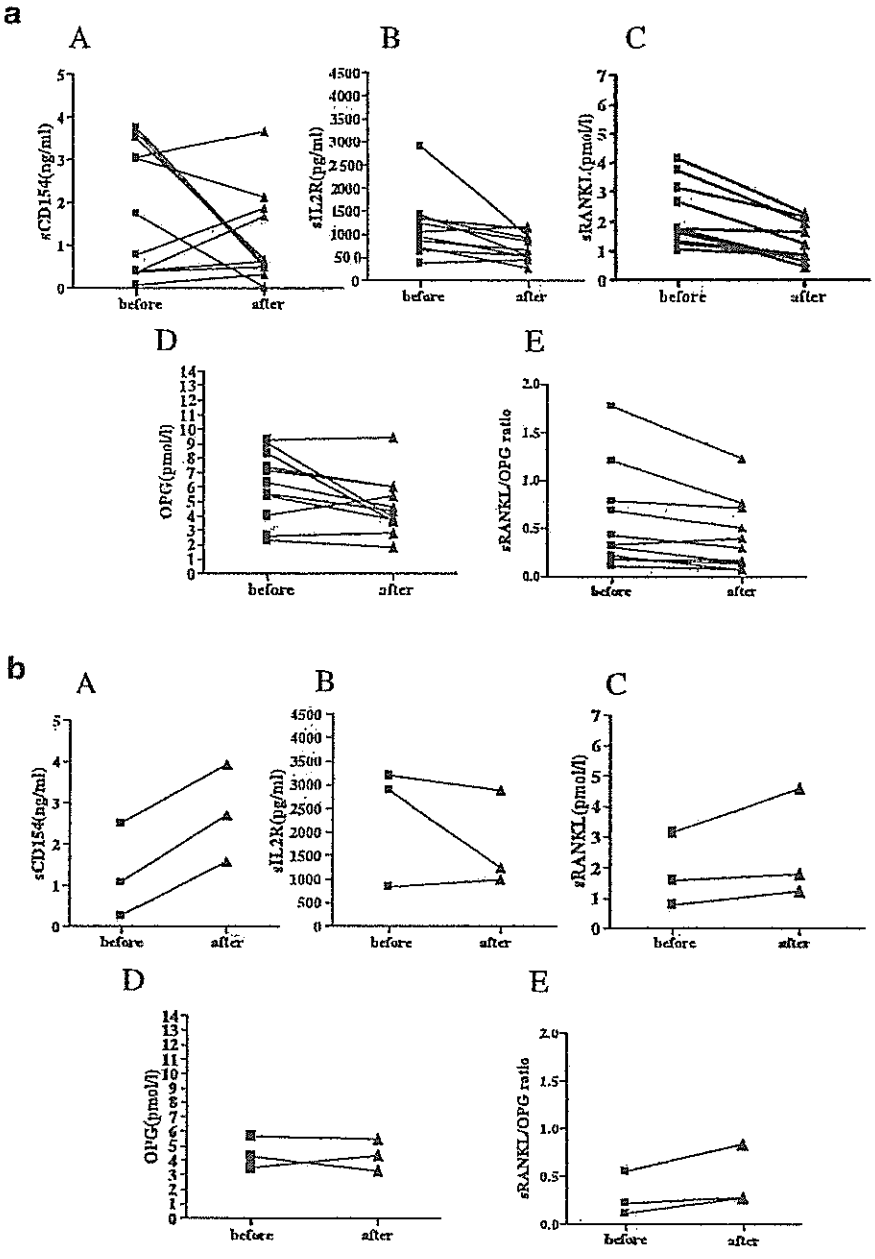

Fig. 4. Serum levels of sCD154, sIL2R, sRANKL, OPG, and sRANKL/OPG ratios in responders (n = 11) (a) and non-responders (n = 3) (b) before and after the induction therapy. A: sCD154; (B) sIL-2R; (C) sRANKL (D) OPG, and (E) sRANKL/OPG ratios.

MM type and in non-responders, while sIL-2R levels improved significantly with treatment in responders. Probably because our assay systems differed from those of Rosso et al. [2], our data showed that serum levels of sIL-2R were only 870 ± 340 pg/ml in the SM type and 2,050 ± 1,060 pg/ml in the MM type and sIL-2R levels were never higher than 5,000 pg/ml in our series. However, the death rate in the study by Rosso et al. [2] was 25.0% (9 of 32 patients) and only 2.2% (1 of 46 patients) in our study, suggesting that more stage-advanced aggressive disease patients might have been included in their series.

During osteoblast–osteoclast interaction in bone, osteoblasts/stromal cells express and secrete RANKL, which binds RANK expressed on the osteoclasts and their precursors. This process promotes maturation and activation of osteoclast. In addition, osteoblasts/stromal cells also secrete OPG, which acts as a decoy receptor and blocks the binding of RANKL to RANK. Outside of bone, RANKL is also expressed and secreted by activated T cells while APCs express RANK and secrete OPG. Thus, the interaction between T cells and APCs enhances activity and survival of these immune cells and modulates bone

absorption [12] and alterations in the sRANKL/OPG ratio are thought to be crucial in the pathogenesis of osteolytic diseases [13,14].

In LCH bone lesions, tumor necrosis factor, interleukin 11, and leukemia inhibitory factor which are potent activators of osteoclast by increasing expression of RANKL are produced by LCH cells [16]. In LCH, osteoclast-like multinucleated giant cells are present in not only the bone but also the non-ostotic lesions, and those cells are activated by M-CSF and RANKL expressed on LCH cells or T cells [17]. Also, in peripheral blood of LCH patients, myeloid dendritic cell precursors were shown to be increased, and the levels of FLT3 ligand and M-CSF promoting the dendritic cell differentiation were elevated [18]. M-CSF and RANKL play a role in differentiating these immature dendritic cells into osteoclasts [19]. Based on these findings, it is reasonable to assume that serum sRANKL/OPG ratios in LCH patients could be altered reflecting metabolic process in the bone lesions. In fact, we found in this study that sRANKL/OPG ratios are significantly higher in LCH patients and are well correlated with the number of LCH bone lesions. Unlike sCD154 levels, sRANKL/OPG ratios in LCH patients may more directly reflect bone metabolic alterations than systemic immune dysfunction. Since clinical evaluation of LCH bone disease activity is difficult, sRANKL/OPG ratios may become a promising clinical marker for that purpose.

In multiple myeloma patients with lytic bone lesions, the serum levels of OPG were reported to be decreased when compared to controls [20], however, in our LCH study, serum OPG levels were found to be higher than controls, especially in MM type LCH patients. The data in LCH could be due to a compensatory self-defense response as immune mechanisms in response to bone destruction lesions. In addition, negative correlation of the serum OPG values and the number of LCH bone lesions in LCH patients may indicate that immunologically uncompensated patients develop severe osteolytic bone lesions. Alternative explanation is that higher levels of OPG may reflect a protection against apoptosis of LCH cells or osteoclasts especially in MM type LCH patients, since OPG can act as a decoy receptor for not only RANKL but also TNF-related apoptosis-inducing ligand (TRAIL), which exerts an anti-apoptotic effect [21]. Future studies determining the correlation between the numbers of osteoclasts or osteoclast-like giant cells in the bone lesions and the serum levels of sRANKL and OPG in each LCH patient may more directly confirm our hypotheses.

With regard to therapeutic implications, pamidronate, an inhibitor of osteoclasts, has been shown to have activity in anecdotal cases of bone lesions in LCH [22]. OPG-Fc fusion protein was more efficacious than pamidronate against multiple myeloma and bone metastases of breast cancer [23]. In the future, sRANKL/OPG ratios may be useful for evaluation of treatment response of LCH bone lesions to novel therapeutic agents.

Based on the current study, we conclude that sIL-2R and sCD154 could be useful as indicators of inflammation and sRANKL/OPG ratios as markers of osteolytic activity. Furthermore, the combination of these systemic biological markers could be useful in evaluating disease activity and/or therapeutic response in the treatment of patients with multi-site LCH.

ACKNOWLEDGMENT

The authors thank members of the Japan LCH Study Group (JLSG) for providing clinical data and samples, and Yasuko Hashimoto for her excellent secretarial assistance.

REFERENCES

1. Schnitz L, Favara BE. Nosology and pathology of Langerhans cell histiocytosis. Hematol Oncol Clin North Am 1998;12:221–246.
2. Rosso DA, Roy A, Zelazko M, et al. Prognostic value of soluble interleukin 2 receptor levels in Langerhans cell histiocytosis. Br J Haematol 2002;117:54–58.
3. Rosso DA, Ripoli MF, Roy A, et al. Serum levels of interleukin-1 receptor antagonist and tumor necrosis factor-alpha are elevated in children with Langerhans cell histiocytosis. J Pediatr Hematol Oncol 2003;25:480–483.
4. Egeler RM, Favara BE, van Meurs M, et al. Differential in situ cytokine profiles of Langerhans-like cells and T cells in Langerhans cell histiocytosis: Abundant expression of cytokines relevant to disease and treatment. Blood 1999;94:4195–4201.
5. Egeler RM, Favara BE, Laman JD, et al. Abundant expression of CD40 and CD40-ligand (CD154) in paediatric Langerhans cell histiocytosis lesions. Eur J Cancer 2000;36:2105–2110.
6. Graf D, Muller S, Korthauer U, et al. A soluble form of TRAP (CD40 ligand) is rapidly released after T cell activation. Eur J Immunol 1995;25:1749–1754.
7. Haswell LE, Glennie MJ, Al-Shamkhani A. Analysis of the oligomeric requirement for signaling by CD40 using soluble multimeric forms of its ligand, CD154. Eur J Immunol 2001; 31:3094–3100.
8. van Kooten C, Banchereau J. CD40-CD40 ligand. J Leukoc Biol 2000;67:2–17.
9. Kato K, Santana-Sahagun E, Rassenti LZ, et al. The soluble CD40 ligand sCD154 in systemic lupus erythematosus. J Clin Invest 1999;104:947–955.
10. Tamura N, Kobayashi S, Kato K, et al. Soluble CD154 in rheumatoid arthritis: Elevated plasma levels in cases with vasculitis. J Rheumatol 2001;28:2583–2590.
11. Heeschen C, Dimmeler S, Hamm CW, et al. Soluble CD40 ligand in acute coronary syndromes. N Engl J Med 2003;348:1104–1111.
12. Hofbauer LC, Schoppet M. Clinical implications of the osteoprotegerin/RANKL/RANK system for bone and vascular diseases. JAMA 2004;292:490–495.
13. Terpos E, Szydlo R, Apperley JF, et al. Soluble receptor activator of nuclear factor kappaB ligand-osteoprotegerin ratio predicts survival in multiple myeloma: Proposal for a novel prognostic index. Blood 2003;102:1064–1069.
14. Hofbauer LC, Neubauer A, Heufelder AE. Receptor activator of nuclear factor-kappaB ligand and osteoprotegerin: Potential implications for the pathogenesis and treatment of malignant bone diseases. Cancer 2001;92:460–470.

15. Schultz C, Klouche M, Friedrichsdorf S, et al. Langerhans cell histiocytosis in children: Does soluble interleukin-2-receptor correlate with both disease extent and activity? Med Pediatr Oncol 1998;31:61–65.
16. Andersson By U, Tani E, Andersson U, et al. Tumor necrosis factor, interleukin 11, and leukemia inhibitory factor produced by Langerhans cells in Langerhans cell histiocytosis. J Pediatr Hematol Oncol 2004;26:706–711.
17. da Costa CE, Annels NE, Faaij CM, et al. Presence of osteoclast-like multinucleated giant cells in the bone and nonostotic lesions of Langerhans cell histiocytosis. J Exp Med 2005;201: 687–693.
18. Rolland A, Guyon L, Gill M, et al. Increased blood myeloid dendritic cells and dendritic cell-poietins in Langerhans cell histiocytosis. J Immunol 2005;174:3067–3071.
19. Rivollier A, Mazzorana M, Tebib J, et al. Immature dendritic cell transdifferentiation into osteoclasts: A novel pathway sustained by the rheumatoid arthritis microenvironment. Blood 2004;104:4029–4037.
20. Seidel C, Hjertner O, Abildgaard N, et al. Nordic Myeloma Study Group. Serum osteoprotegerin levels are reduced in patients with multiple myeloma with lytic bone disease. Blood 2001;98:2269–2271.
21. Colucci S, Brunetti G, Rizzi R, et al. T cells support osteoclastogenesis in an in vitro model derived from human multiple myeloma bone disease: The role of the OPG/TRAIL interaction. Blood 2004;104:3722–3730.
22. Farran RP, Zaretski E, Egeler RM. Treatment of Langerhans cell histiocytosis with pamidronate. J Pediatr Hematol Oncol 2001; 23:54–56.
23. Body JJ, Greipp P, Coleman RE, et al. A phase I study of AMGN-0007, a recombinant osteoprotegerin construct, in patients with multiple myeloma or breast carcinoma related bone metastases. Cancer 2003;97:887–892.

Original Article

Cytogenet Genome Res 115:51–61 (2006)
DOI: 10.1159/000094801

Cytogenetic and Genome Research

Genomic structure of swine taste receptor family 1 member 3, *TAS1R3*, and its expression in tissues

S. Kiuchi[a] T. Yamada[b] N. Kiyokawa[c] T. Saito[a] J. Fujimoto[c] H. Yasue[a]

[a]National Institute of Agrobiological Sciences, Tsukuba, Ibaraki
[b]School of Medicine, Keio University, Shinjuku-ku
[c]National Research Institute for Child Health and Development, Setagaya-ku, Tokyo (Japan)

Manuscript received 18 October 2005; accepted in revised form for publication by H. Hameister, 9 February 2006.

Abstract. Taste receptor family 1 member 3, TAS1R3, is shown to be involved in sweet and umami tastes in mouse, and the nucleotide sequence of the gene has been reported in rat, gorilla, and human. Pigs are frequently used as models for human diseases, and are also considered to be source animals for xenotransplantation to humans due to their anatomical and physiological similarities to humans. Therefore, in the present study, the genomic structure of the swine *TAS1R3* gene was determined, and *TAS1R3* expression was studied in various swine tissues. The gene was shown to reside on swine chromosome 6q22→q23, from which three types of mRNAs were generated: 3,752 bp derived from six exons in tongue, 3,704 bp from six exons and 3,630 bp from seven exons in testis. The 6 exons/5 introns were structurally similar to those of humans and mice, but the 7 exons/6 introns structure of *TAS1R3* was first observed in swine. High expressions of *TAS1R3* were revealed in tongue, kidney, and testis by real-time PCR. The expression profile of the tissues except for kidney was similar to that of mouse. When in situ hybridization using an RNA probe for *TAS1R3* was performed on swine tongue and testis tissues, *TAS1R3* expressions were revealed in tongue circumvallate papillae, fungiform papillae, mucosal epithelium, follicular B lymphocytes, lymphocytes in submucosal tissues of lingual tonsil, and spermatogenic cells. Using peripheral mature B lymphocytes, the expression of *TAS1R3* in B lymphocytes was further confirmed by real-time PCR and sequencing of the real-time PCR product.

Taste consists of five modalities, that is, salty, sour, bitter, sweet, and umami. These modalities are necessary for growth and survival in animals. Physiological studies have indicated that taste receptor cells selectively respond to different tastants (Gilbertson et al., 1992; Bernhardt et al., 1996; Cummings et al., 1996). Electro-physiological studies have suggested that salty and sour tastants modulate taste receptor cell function by directly affecting specialized membrane channels (Kretz et al., 1999; Lin et al., 2004). On the other hand, taste responses to bitter, sweet, and umami are shown to be initiated by G-protein-coupled receptors (GPCRs) and transduced via G-protein signaling cascades (Gilbertson et al., 2000; Lindemann, 2001). Bitter tastants are detected by ~30 members of the taste receptor family 2 (TAS2R), a subfamily of the GPCRs. Most TAS2Rs are co-expressed in the same subset of taste receptor cells (Adler et al., 2000), suggesting that these cells function as generalized bitter detectors. Sweet and umami tastes are mediated by three members of the taste receptor family 1 (TAS1R), a distinct GPCR subfamily. TAS1Rs combine to assemble two heteromeric GPCR complexes. The complex of taste receptor family 1 member 2 (TAS1R2) and taste receptor family 1 member 3 (TAS1R3) serves as a sweet taste receptor (Nelson et al., 2001; Li et al., 2002; Zhao et al., 2003); and that of

Request reprints from Hiroshi Yasue
Genome Research Department
National Institute of Agrobiological Sciences, 2 Ikenodai
Tsukuba, Ibaraki 305-0901 (Japan)
telephone: +81-298-38-8664; fax: +81-298-38-8674
e-mail: hyasue@affrc.go.jp

KARGER Fax +41 61 306 12 34
E-Mail karger@karger.ch
www.karger.com

1424–8581/06/1151–0051$23.50/0

Accessible online at:
www.karger.com/cgr

taste receptor family 1 member 1 (TAS1R1) and TAS1R3, as an umami taste receptor (Li et al., 2002; Nelson et al., 2002; Zhao et al., 2003). In the genetic analysis of mice strains showing differences in preference for sweet, it is suggested that the sequence polymorphisms causing amino-acid substitutions are associated with this preference (Max et al., 2001; Reed et al., 2004).

Recently, pigs have drawn the attention of many researchers not only as a model animal for human diseases but also as a resource for xenotransplantation to humans because of their anatomical and physiological similarities to humans (Tumbelson and Schook, 1996). In line with this and the fact that elucidation of the preferences in pig populations would help breeding in terms of feeding efficiency (one of the major factors in animal science), in the present study we have determined the genomic structure of swine *TAS1R3* and investigated the mode of *TAS1R3* gene expression in various tissues. The swine *TAS1R3* gene is similar to that of human and mouse with respect to its reported genome structure and expression. Furthermore, the present study for the first time has revealed an alternative splicing of *TAS1R3* in testis and *TAS1R3* expression in tongue mucosal epithelium, mature B lymphocytes, and spermatogenic cells. This may imply as yet unreported additional functions of TAS1R3.

Materials and methods

Pigs for preparation of tissues and cells

Three and a half month-old male pigs of Landrace or Landrace/Duroc/Largewhite composite were used to obtain tissue for both RNA and in situ gene expression analyses. The animals used in the present study received humane care as described in the Guidelines for the Care and Use of Experimental Animals (National Institute of Agrobiological Sciences Care Committee, Japan). Peripheral blood cells obtained from these pigs were applied to a cell-sorter (EPICS ALTRA; Beckman Coulter, CA, USA) using anti-CD21 antibody (VMRD, Inc., WA, USA) to obtain a mature B lymphocyte population. The process for the preparation of tissue samples followed the guidelines of animal ethics at the National Institute of Agrobiological Sciences. The pigs were euthanized by an intravenous injection of 10 ml of sodium pentobarbital. Immediately after respiration and heartbeat stopped, tissue samples were excised from tongue, heart, lung, stomach, intestine, liver, kidney, and testis to prepare RNA and to fix tissues in 4% (w/v) paraformaldehyde in phosphate-buffered saline.

Analysis of swine TAS1R3 gene structure

To obtain bacterial artificial chromosome (BAC) clones containing the *TAS1R3* gene, a swine genomic DNA BAC library constructed by Suzuki et al. (2000) was screened by PCR. Primers (forward: hT1R3-Ex2L, reverse: hT1R3-Ex2R in Table 1) for PCR were designed from the human sequence (GenBank/EMBL/DDBJ Data Bank Accession No. BK000152) showing a high similarity to the mouse *Tas1r3* sequence (Accession No. AF337039, AL670236.9). The fragment (200 bp) amplified from swine genomic DNA by PCR using the primers was sequenced to confirm that the sequence was orthologous to that of human *TAS1R3*. BAC clones were subsequently selected from the library, and the purified BAC-DNA was cleaved with *Hin*dIII, fractionated by electrophoresis, and hybridized with a digoxigenin-labeled swine DNA fragment amplified by the above primers (PCR DIG Probe Synthesis Kit: Roche Diagnostics, Mannheim, Germany). BAC-DNA fragments which hybridized to the digoxigenin-labeled fragment were subcloned into pBluescript KS(+) and sequenced using PRISM Ready Reaction BigDye Terminator Cycle Sequencing Kits (ver. 2) (Applied Biosystems, Calif., USA) and an ABI3100 DNA sequencer (Applied Biosystems).

Preparation of porcine RNA

RNA was prepared from 0.7–1.7 g tissue samples using the guanidinium thiocyanate acid-phenol-chloroform method with TRIzol reagent (Invitrogen, Calif., USA) and from the mature B lymphocytes using RNeasy (QIAGEN Sciences, Md., USA). The RNAs thus prepared were treated with DNase I (TAKARA, Shiga, Japan) at 37°C for 30 min, and then with phenol:chloroform. The amounts and purities of the resulting RNAs were estimated by their absorbance from 220 to 320 nm.

Analysis of TAS1R3 cDNA

First-strand cDNA was prepared from the RNA obtained by the above, following the procedure described by Suzuki and Sugano (2003), and then used to amplify the *TAS1R3*-specific DNA fragments by PCR using primer pairs (see Table 1) designed with a swine *TAS1R3* genomic sequence. Briefly, PCR was performed in a 50 μl reaction mixture containing 2 μl of the tongue or testis first-strand cDNA as a template, LA PCR buffer (without $MgCl_2$) (TAKARA), 1.5 mM $MgCl_2$, 400 μM dNTPs, 0.05 U/μl TaKaRa LA Taq (TAKARA) and 0.2 μM primer pair (forward: T1R3-ExStaF, reverse: T1R3-3R), as indicated in Table 1. PCR was carried out at 94°C for 1 min, followed by 40 cycles of PCR consisting of 30 s denaturation at 94°C, 30 s annealing at 60°C, and 4 min extension at 72°C, and finally an extension step at 72°C for 10 min. Secondary PCR was performed using an aliquot of the preceding PCR product and a nested pair of primers (forward: T1R3-ExStaF, reverse: T1R3-ExEndR) (Table 1). Amplified PCR fragments were cloned into pUC118 and sequenced by the primer-walking method.

In order to obtain the 5′ and 3′ terminal regions of the *TAS1R3* transcripts, 5′ and 3′ rapid-amplification-of-cDNA ends (RACE) analysis was performed with the 5′/3′ RACE kit (Roche Diagnostics), following the manufacturer's instructions. The primer pairs for the RACE analysis are described in Table 1. The DNA fragments obtained by the RACE analysis were cloned and sequenced as above.

Attempts to identify SNPs (single nucleotide polymorphisms) of TAS1R3 possibly related to tasting

The genomic DNAs of a swine from each of five breeds, viz, Göttingen, Largewhite, Duroc, Berkshire, and Japanese wild boar, two from Landrace, and two F_1 from a Meishan × Göttingen cross population (Mikawa et al., 1999) were sequenced to identify sequence polymorphisms for the sweet preference, as in mouse (Max et al., 2001; Reed et al., 2004).

Assignment of TAS1R3 to the IMpRH map

In order to assign *TAS1R3* to the IMpRH map (http://imprh.toulouse.inra.fr/), primer pairs were designed in the sequence of *TAS1R3* and examined to select those which amplified the expected sequences from swine genomic DNA but not from Chinese hamster genomic DNA. One of the primer pairs (forward: H6-2-R2, reverse: T1R3-Ex1R in Table 1) was used for typing of IMpRH panel DNAs which had been kindly provided by INRA (France) and the University of Minnesota (USA) for radiation hybrid (RH) mapping (Yerle et al., 1998). The typing procedure was the same as that described previously (Kiuchi et al., 2002). The typed data were submitted to the IMpRH server at http://imprh.toulouse.inra.fr/ (Milan et al., 2000) to obtain the likely position of *TAS1R3* on the IMpRH map.

Fluorescence in situ hybridization localization of TAS1R3 on swine chromosome

Swine peripheral blood cells (Landrace) were cultured and labeled with 5-BrdU as described previously (Awata et al., 1995). The cultured cells were treated with hypotonic solution and fixative, followed by spreading on glass slides as described previously (Yasue and Ishibashi, 1982). Chromosome spreads were then subjected to FISH as described previously (Awata et al., 1995) using probe DNA. For the probe DNA, BAC DNA (500 ng) containing the *TAS1R3* gene was labeled with biotin using a nick translation kit (Roche Diagnostics).

Table 1. Primer list

Project / Primer name	Primer positions[a] from / to	Sequence (5'–3')	Size (mer)	Annealing temperature (°C)	PCR product size (bp)
BAC library screening /					
hT1R3-Ex2L (forward)		CTACGACCTCTTTGATACGTGCTC	24	61	200
hT1R3-Ex2R (reverse)		GCATGAGGAAGAAGCTGAAGAACT	24		
1st-PCR for cDNA cloning /					
T1R3-ExStaF (forward)	–37 / –16	TGCTCACTGCCATCCCTGCTGG	22	60	3,321
T1R3-3R (reverse)	+3828 / +3807	ACCCATGACTGGCTTGGTACTG	22		
2nd-PCR for cDNA cloning /					
T1R3-ExStaF (forward)	–37 / –16	TGCTCACTGCCATCCCTGCTGG	22	60	2,627
T1R3-ExEndR (reverse)	+3134 / +3113	GGCACCTTGACTACGTCTGAGG	22		
Synthesis of 1st-strand cDNA in 5'RACE /					
T1R3-Ex3R	+701 / +682	GAAGAAGGAGGGGAACGTCT	20		
1st-PCR in 5'RACE /					
Oligo dT-anchor primer (forward) (Roche)		GACCACGCGTATCGATGTCGACTTTTTTTTTTTTTTTV	39	57	
T1R3-Ex2R3 (reverse)	+541 / +522	AGCCGAAGAACTTGCCGGTG	20		
2nd-PCR in 5'RACE /					
PCR anchor primer (forward) (Roche)		GACCACGCGTATCGATGTCGAC	22	59	
T1R3-Ex1R (reverse)	+104 / +84	AGCACGTAGTGCCCTTGCATG	21		
1st-PCR in 3'RACE /					
T1R3-Ex67F (forward)	+2839 / +2859	CATGCTGGCCTACTTCATCAC	21	57	
PCR anchor primer (reverse) (Roche)		GACCACGCGTATCGATGTCGAC	22		
2nd-PCR in 3'RACE /					
T1R3-Ex67F2 (forward)	+2967 / +2986	ACCTGCCCAAGTGCTACCTG	20	59	
PCR anchor primer (reverse) (Roche)		GACCACGCGTATCGATGTCGAC	22		
RH mapping /					
H6-2-R2 (forward)	–203 / –182	GGTGGCATCAGAATAAGAGTCC	22	59	307
T1R3-Ex1R (reverse)	+104 / +84	AGCACGTAGTGCCCTTGCATG	21		
Real-time PCR for *TAS1R3* /					
tg-502T (TaqMan probe)		CCACCGTGTGTACCAGGTTCTCGTC	25		
tg-476F (forward)	+144 / +160	GCTGGGCGACAGGACAG	17	50	102
tg-577R (reverse)	+317 / +298	TTGATTTCCTCCACAGCCAT	20		
RNA synthesis from *EGFP* /					
T7p-EGFP-540F (forward)		AGTAATACGACTCACTATAGGGCGACCACTACCAGCAGAACA	42	59	218
dT18-EGFP-717R (reverse)		TTTTTTTTTTTTTTTTTTCTTGTACAGCTCGTCCATGC	38		
Real-time PCR for *EGFP* /					
FAM-EGFP-634T (TaqMan probe)		CCCAACGAGAAGCGCGATCACA	22		
U57608EGFP615F (forward)		GTCCGCCCTGAGCAAAGA	18	50	62
U57608EGFP676R (reverse)		TCACGAACTCCAGCAGGACC	20		
Synthesis of ISH Anti-Sense cRNA probe /					
T1R3-71F (forward)	+2854 / +2873	CATCACCTGGGTTTCCTTTG	20	57	165
T7-prm-T1R3-72R (reverse)	+2996 / +2977	AGTAATACGACTCACTATAGGGACCTCAGCAGCAGGTAGCAC	42		
Synthesis of ISH Sense cRNA probe /					
T7-prm-T1R3-71F (forward)	+2854 / +2873	AGTAATACGACTCACTATAGGGCATCACCTGGGTTTCCTTTG	42	57	165
T1R3-72R (reverse)	+2996 / +2977	ACCTCAGCAGCAGGTAGCAC	20		

[a] Positions based on the nucleotide number shown in Fig. 1.

Measurement of TAS1R3 gene expression by real-time PCR

An aliquot of each RNA sample was mixed with an amount of RNA fragment synthesized from pEGFP-C1 vector (EGFP: enhanced green fluorescent protein, Invitrogen), and the resulting mixture was subjected to synthesis of the first-strand cDNA using SuperScript III (Invitrogen), 5 μM Random Hexamer and 500 μM dNTPs, following the manufacturer's procedure. The RNA fragment from EGFP was prepared using a primer pair (forward: T7p-EGFP-540F, reverse: dT18-EGFP-717R in Table 1) with the AmpliScribe T7 High Yield Transcription Kit (EPICENTRE, Wisc., USA), and was then used as a monitor for reverse transcription efficiency and a standard for a quantitative comparison of *TAS1R3* transcripts among the samples. Samples subjected to synthesis of the first-strand cDNA were treated with RNaseH (TOYOBO, Osaka, Japan) at 37°C for 20 min. First-strand cDNA derived from *TAS1R3* transcripts in the samples was detected using TaqMan Universal Master Mix (Applied Biosystems), TaqMan probe (tg-502T) and the primer pair (forward: tg-467F, reverse: tg-557R), according to the procedure recommended by Applied Biosystems (ABI 7700). The first-strand cDNA derived from EGFP RNA was detected using TaqMan Universal Master Mix (Applied Biosystems), TaqMan probe (FAM-EGFP-634T) and a primer pair (forward: U57608EGFP615F, reverse: U57608EGFP676R). Primer sequences are listed in Table 1.

Prior to measurement, the fragment amplified from the tongue sample with the primer pair for *TAS1R3* was sequenced to confirm that

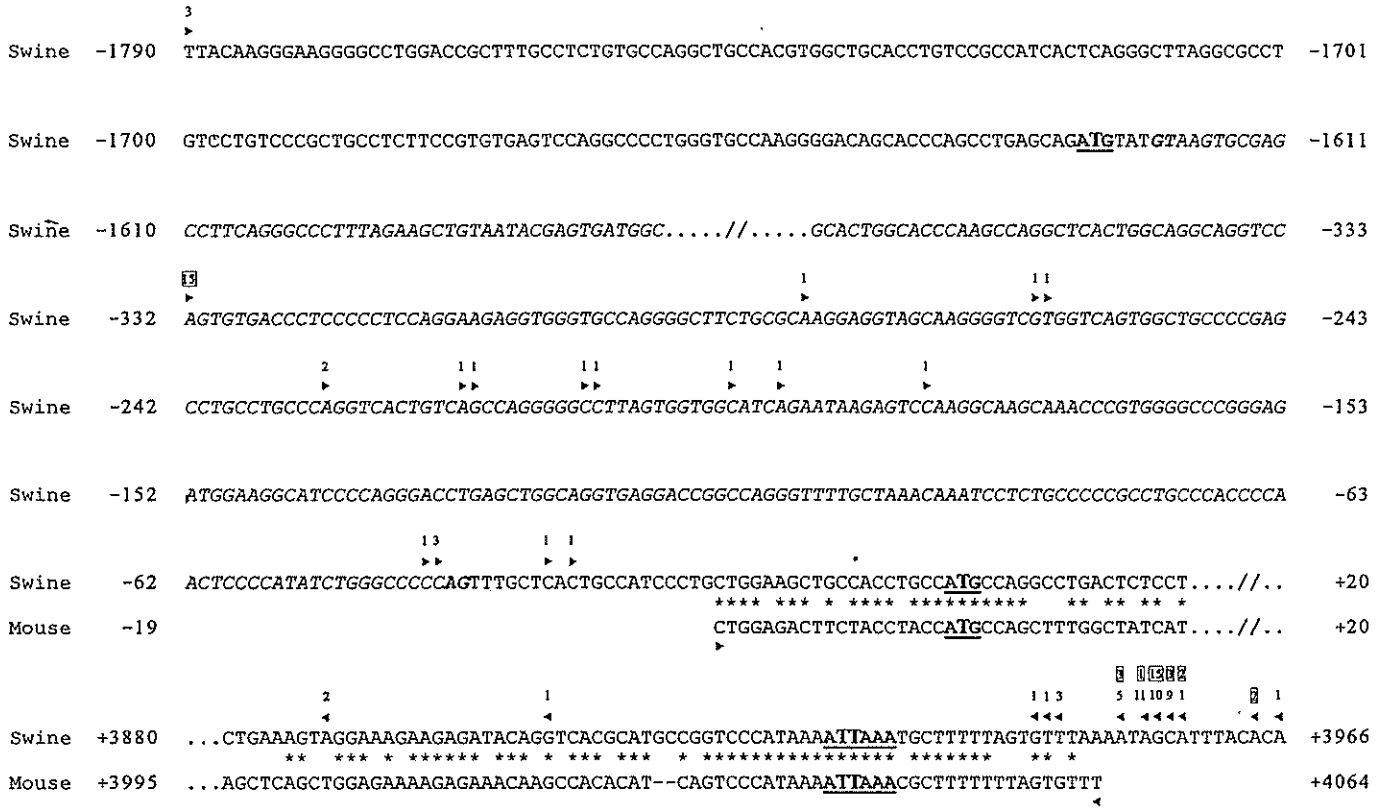

Fig. 1. Transcription initiation and termination sites of swine *TAS1R3*. The *TAS1R3* genomic sequence was numbered downstream of the transcription with the putative translation start site of Tongue1 as +1. That start site and polyadenylation signal site are denoted by bold letters and underlines. The sequence indicated to be the intron for Tes2 transcription is shown in italics. Downstream arrowheads with boxed and unboxed numerals indicate initiation sites of the transcription in tongue and testis, respectively. Upstream arrowheads with boxed and unboxed numerals indicate termination sites of the transcription in tongue and testis, respectively. The numerals represent the number of clones showing initiation or termination of the transcription at the site of each arrowhead in the RACE analysis. As a reference, part of the mouse sequence was aligned with a swine sequence to show the transcription initiation and termination sites reported in mouse (Accession No. AF337039 and AL670236.9).

the primer pair amplified the expected sequence. In addition, it was confirmed that the DNA fragment from EGFP RNA was proportionally amplified depending on the amount of EGFP RNA used for real-time PCR.

Detection of gene expression site in tissues by in situ hybridization

After dissected tissues were fixed overnight in paraformaldehyde solution, they were embedded in paraffin and then sectioned 4 μm thick. Sections were collected on glass-slides and subjected to in situ hybridization. The procedure for in situ hybridization was the same as that reported earlier (Ohtsuki et al., 1998) with the following exception: hybridization was performed in a solution containing 50% formamide, 2× SSC, 1.0 mg/ml tRNA, 1.0 mg/ml salmon sperm DNA, 1.0 mg/ml BSA, 10% dextran sulfate, 1.0% SDS, and 8.0 μg/ml RNA anti-sense or sense probe at 37°C for 16 h. Hybridization signals were detected with the NBT/BCIP system (Sigma-Aldrich, Mo., USA).

For the RNA probe, DNA fragments were first prepared by PCR from *TAS1R3* cDNA using primer pairs T1R3-71F:T7-prm-T1R3-72R, and T7-prm-T1R3-71F:T1R3-72R. The sequences of primers are listed in Table 1. Using the DNA fragment obtained with the primer pair T1R3-71F:T7-prm-T1R3-72R and using the AmpliScribe T7-Flash Transcription Kit (EPICENTRE), a digoxigenin-labeled RNA anti-sense probe was prepared according to the manufacturer's instructions. With the same procedure, a digoxigenin-labeled RNA sense probe was prepared using the DNA fragment obtained with the primer pair T7-prm-T1R3-71F:T1R3-72R.

Results

TAS1R3 gene

A swine genomic DNA BAC library was screened to obtain three BAC clones containing at least a part of the putative *TAS1R3* gene. DNA from the BAC clones was processed as described in Material and methods to identify a *Hin*dIII fragment (about 6.6 kb) that contained the putative *TAS1R3* gene. The 6.6 kb fragment of one BAC clone (code 994D12) was cloned in pBluescript KS(+) and sequenced. In addition, cDNA fragments (2,627 bp) of *TAS1R3* transcripts from tongue tissue were generated using the primer pairs listed in Table 1, cloned into pUC118 vector, and sequenced. Since 5′/3′ regions of the putative *TAS1R3* gene transcript were likely to be missing from the cDNA sequences, RACE analysis was performed using the RNA prepared from tongue to determine the sequences of the 5′/3′ terminal regions. Fifteen fragments obtained by 5′ RACE were sequenced, revealing that all the transcriptions initiated from nucleotide position –332 (numbered from the translation start nucleotide in the 3′-direction in the present study). The sequenc-

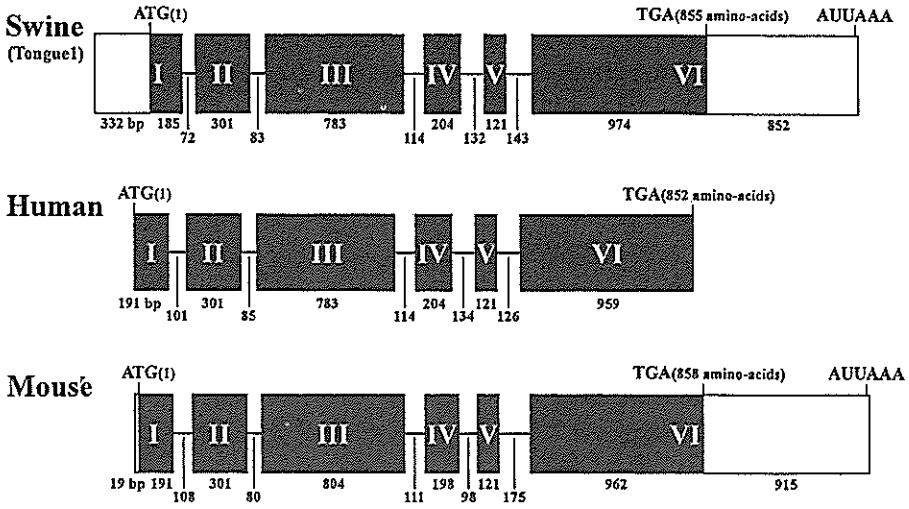

Fig. 2. Schematic presentation of swine *TAS1R3* gene structure. Boxes denote exons, with white parts representing 5′-untranslated region (UTR) and 3′UTR; and black parts signifying protein-coding regions. Exons are numbered according to their correspondence with those of human and mouse. As a reference, the genomic structures of human and mouse *TAS1R3* genes are included in this figure. The accession numbers for human and mouse cDNA of *TAS1R3* genes are BK000152 and AF337039, respectively. Those for human and mouse genomic DNA are NT_077965.1 and AL670236.9, respectively.

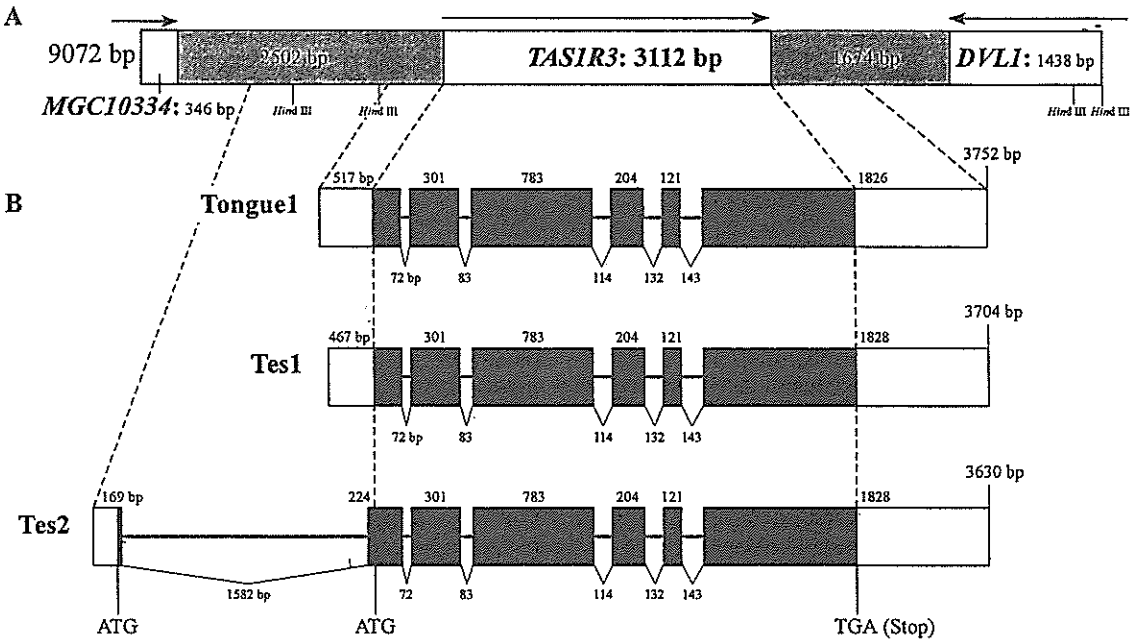

Fig. 3. Correspondence of swine *TAS1R3* transcripts to genomic sequence. (**A**) Swine genomic structure of the region encompassing *TAS1R3*. Regions tagged with *MGC10334* and *DVL1* correspond to human *MGC10334* and *DVL1*, respectively, based on sequence similarities. (**B**) Swine *TAS1R3* genomic structures, from which *TAS1R3* transcripts, Tongue1, Tes1, and Tes2, were derived. The reconstituted longest transcript in each type is presented in this figure. Symbols and markings in this figure are the same as those in Fig. 2.

ing of 26 fragments in 3′ RACE demonstrated that the transcriptions terminated at the nucleotide positions ranging from +3953 to +3964 (Fig. 1).

The reconstituted longest cDNA sequence (3,752 bp; from −332 to +3964 of the swine genomic sequence) (Tongue1: Accession No. AB162127) was then compared with the swine genomic sequence determined in the present study, revealing that swine putative *TAS1R3* consists of six exons and five introns, spanning 4,296 bp (Accession No. AB162126) (Fig. 2). When the structure of the putative *TAS1R3* gene was compared with those of human and mouse *TAS1R3* genes, it was found that their genomic structures were the same, though slight differences in the lengths of exons and introns were observed (Fig. 2). When the protein-coding sequence of Tongue1 was compared with that of human and mouse, the similarities between swine and human, and between swine and mouse were found to be 81.1% and 73.9%, respectively. These findings taken together led us to

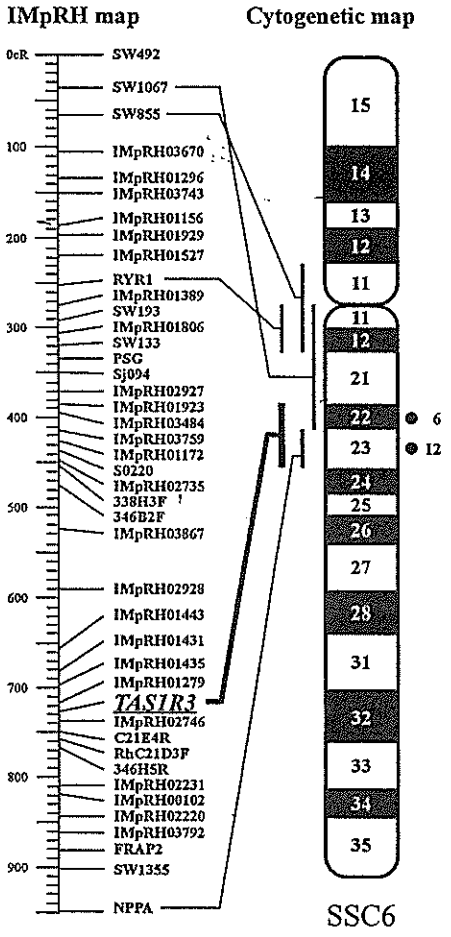

Fig. 4. Chromosomal location of swine *TAS1R3*. The position of *TAS1R3* (shown with italic and underline) on the IMpRH map was indicated. *TAS1R3* was assigned to the map by the RH mapping procedure described in Materials and methods (http://imprh.toulouse.inra.fr/). In addition, the chromosomal position of *TAS1R3* was determined by FISH, also described in Materials and methods. Hybridization signals obtained in FISH were scored along bands of the SSC6 ideogram, and presented as closed circles with the number of signals scored.

conclude that this swine putative *TAS1R3* gene is the orthologue of human and mouse *TAS1R3* genes.

Max et al. (2001) observed that *TAS1R3* mRNA of mouse testis showed a size difference from that of mouse tongue. Therefore, swine *TAS1R3* mRNA derived from testis was examined as in the case of tongue mRNA. This analysis revealed that two types of mRNA were generated from the *TAS1R3* gene in testis: one (Tes1: Accession No. AB162128) was the same as the tongue type, except that its transcription initiation sites varied in range from −282 to −31; the other (Tes2: Accession No. AB162129) contained an additional 45-bp protein-coding sequence upstream from the translation start site observed in Tongue1 and Tes1, which provided an additional 15 amino-acids to the deduced TAS1R3 protein encoded by Tongue1 and Tes1. The transcription termination sites of Tes2 were found to be similar to those of Tongue1 and Tes1. In order to determine the genomic structure for Tes2 production, the BAC-DNA was additionally sequenced, and compared with Tes2 sequences. It was revealed that Tes2 was derived from seven exons, which is the result of alternative splicing of *TAS1R3* as shown in Fig. 3.

Chromosomal assignment of TAS1R3

The swine genomic sequence containing *TAS1R3* (Accession No. AB162126) was compared with the corresponding human and mouse sequences. That comparison demonstrated that the arrangement of genes, i.e., *MGC10334-TAS1R3-DVL1* in swine (Fig. 3A), was the same as that of human and mouse, showing that the genomic region encompassing *TAS1R3* has been conserved at least in those three species. RH mapping was performed to assign the gene to the IMpRH map of swine chromosome (SSC) 6 between IMpRH01279 and IMpRH02746 (Fig. 4). We also carried out FISH to locate the gene physically on SSC6. FISH, as shown in Fig. 4, demonstrated that *TAS1R3* resides on SSC6q22→q23; this result is consistent with that of RH mapping.

Amino-acid sequence of TAS1R3

The amino-acid sequences derived from Tongue1 (or Tes1) and Tes2 were aligned with human and mouse TAS1R3 (Fig. 5). Based on the annotation of human and mouse TAS1R3, a signal peptide (http://www.cbs.dtu.dk/services/SignalP/), an ANF-receptor domain (receptor family ligand binding region), and a 7tm_3 domain (metabotropic glutamate family) (http://www.ncbi.nlm.nih.gov/BLAST/) were identified in the swine TAS1R3 amino-acid sequence of the alignment (Fig. 5).

When swine TAS1R3 derived from Tongue1 (or Tes1) was compared with that of human and mouse, the overall similarities of TAS1R3s between swine and human and between swine and mouse were calculated to be 75.1% and 71.6%, respectively. The similarities between swine and human, and between swine and mouse for the signal peptide region were calculated to be 47.1% and 50.0%, respectively, while those for the ANF-receptor domain were 74.5% and 72.6%, and those for the 7tm_3 domain were 81.7% and 76.6%, respectively. The borders between exons for swine, human, and mouse all occurred at the same positions in the alignment shown in Fig. 5, which is additional evidence for the similarity of the *TAS1R3* gene among the three species.

Since an additional 15 amino-acids were observed at the N-terminus of the protein derived from Tes2 compared to that from Tongue1 (or Tes1), the deduced amino-acid sequence from Tes2 was subjected to a web analysis for signal

Fig. 5. Alignment of swine, human and mouse TAS1R3 amino-acid sequences. The protein deduced from Tongue1/Tes1 comprises 855 amino-acids, and that from Tes2 870 amino-acids. Amino-acid sequences of proteins were aligned with human and mouse TAS1R3 using Genetyx (Software Development Co., Ltd., Tokyo, Japan). The amino-acids of Tes2 identical to those of Tongue1/Tes1 are shown by dots.

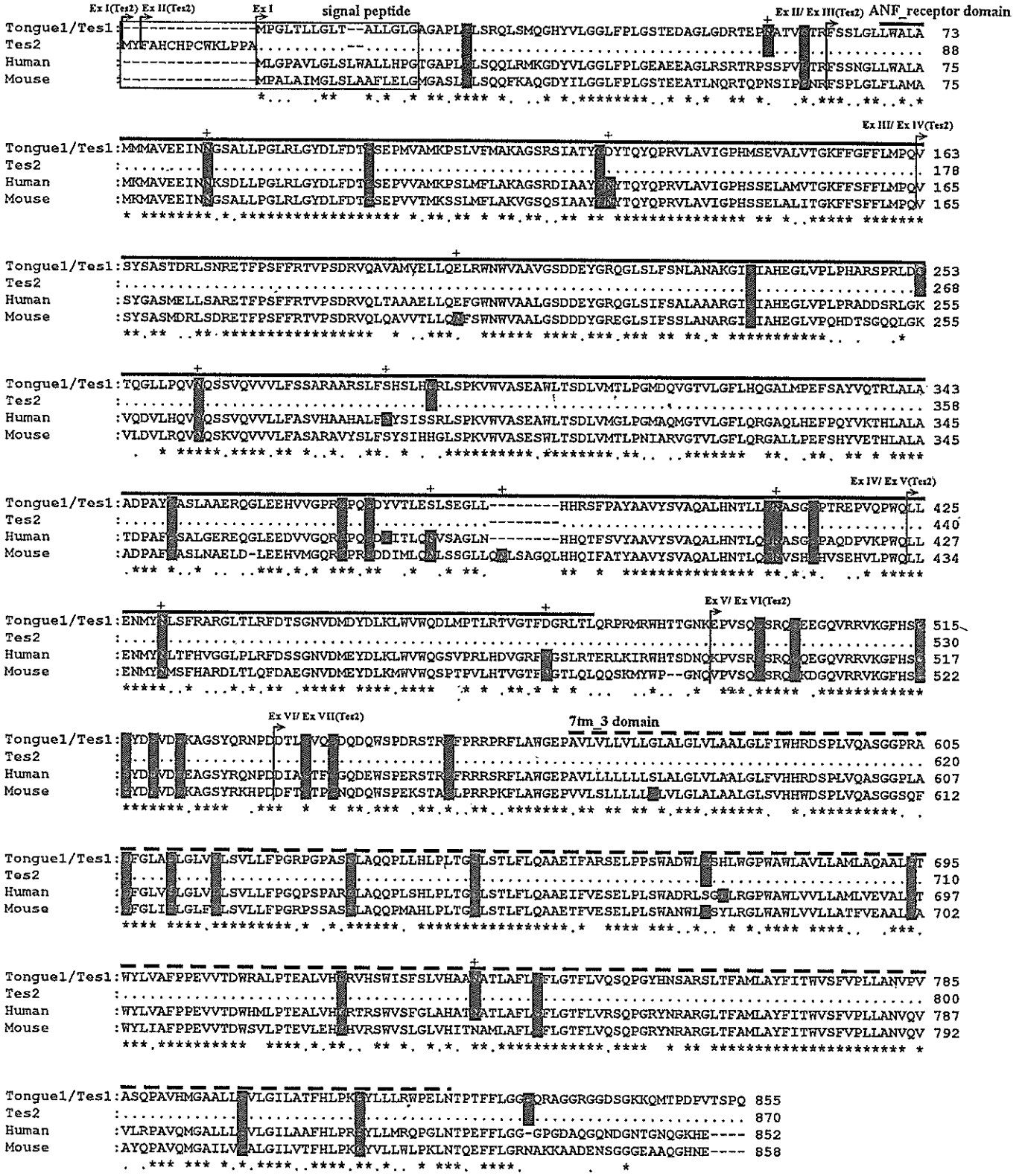

Putative signal peptide (http://www.cbs.dtu.dk/services/SignalP/) is boxed. The putative ANF-receptor domain (http://www.ncbi.nlm.nih.gov/Structure/cdd/cddsrv.cgi?uid=pfam01094&version=v2.04) and putative seven transmembrane domain (7tm_3 domain; http://www.ncbi.nlm.nih.gov/Structure/cdd/cddsrv.cgi?uid=pfam00003&version=v2.04) are marked by the solid and broken lines over the sequence, respectively. Potent N-linked glycosylation sites and cysteine residues are indicated by gray boxes with and without '+', respectively. Amino-acids conserved among swine, human, and mouse in the alignment are indicated by asterisks. Four out of six potent N-linked glycosylation sites and 29 out of 33 cysteine residues in swine are conserved in the three species.

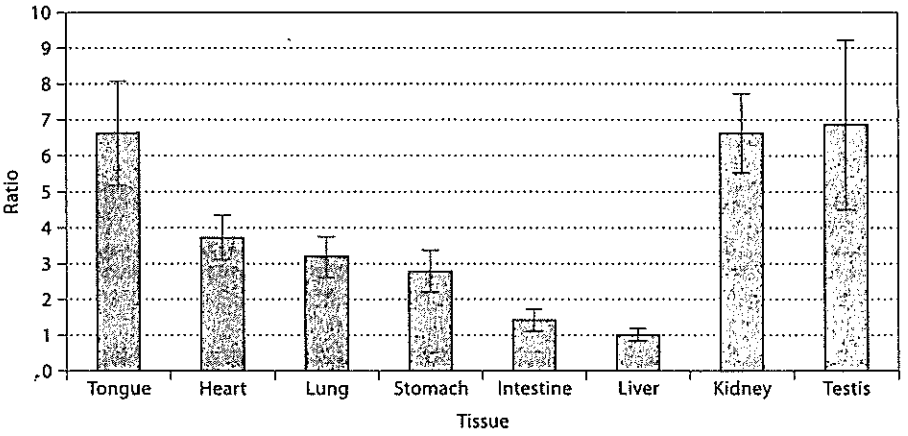

Fig. 6. Measurement of *TAS1R3* gene expressions in tissues by real-time PCR. RNA was prepared from tongue, heart, lung, stomach, intestine, liver, kidney, and testis, and subjected to real-time PCR as described in Materials and methods. Eight real-time measurements were made for each tissue sample, and mean values and standard errors were calculated for each sample. Values thus obtained were recalculated taking the mean value of liver as 1.0, and resulting values were plotted in this figure.

peptide (http://www.cbs.dtu.dk/services/SignalP/). The entire region of 33 consecutive amino-acids (i.e., 15 amino-acids plus the 18 amino-acid sequence corresponding to the signal peptide of the protein from Tongue1) at N-terminus of the protein from Tes2, was recognized as signal peptide. Therefore it is likely that TAS1R3 generated from Tes2 is functionally identical to those from the other transcripts.

DNA sequences of possible control region for TAS1R3

Since the 346 bp at the 5′ terminus of the 2,848-bp segment located upstream of the *TAS1R3* translation start site was indicated to be a part of a gene corresponding to human *MGC10334* or mouse *BC002216* (orthologue of human *MGC10334*) (http://www.ncbi.nlm.nih.gov/BLAST/) (see Fig. 3A), the sequence of the segment excluding the 346 bp was compared with the corresponding human and mouse sequences. The comparison indicated that the swine sequence from the translation start site to 317 bp upstream of the start site (designated as 317 bp sequence) showed a similarity to the corresponding human and mouse regions. The swine 317 bp sequence was then subjected to analysis of transcription factor binding sites (http://www.cbrc.jp/research/db/TFSEARCHJ.html), which revealed SRY and GATA-1/GATA-2 binding sites in the region (data not shown). The SRY binding site was also found in the corresponding human and mouse regions. When the swine sequence excluding the 317 bp and 346 bp sequences was subjected to the analysis of transcription factor binding sites using the above website, the analysis demonstrated 43 transcription factor binding sites, none of which, however, were commonly found in the corresponding human and mouse sequences (data not shown). These findings taken together indicated that the SRY binding site in the 317 bp sequence might function to control the transcription of *TAS1R3*.

Expression of TAS1R3 in swine tissues

The expression of *TAS1R3* in swine was investigated in tongue, heart, lung, stomach, intestine, liver, kidney, and testis by real-time PCR (Fig. 6), the results of which were normalized with reference to the amount of EGFP RNA added as a control along with the RNA samples. Tongue, kidney, and testis expressed the *TAS1R3* gene at a much higher rate than other tissues (Fig. 6). It was also demonstrated that heart, lung, and stomach expressed the gene significantly more than intestine and liver, though the extent of the elevations was small. The feature of *TAS1R3* gene expression in swine tissues examined was found to be essentially the same as that for mouse except that kidney expressed the gene as much as tongue in swine.

Determination of TAS1R3 gene expression sites in tissues

In order to investigate the localization of *TAS1R3* gene expression within various tissues, tongue, testis, and kidney were subjected to in situ hybridization using the RNA probes derived from exon 6. As shown in Fig. 7, tongue was found to express the gene in the circumvallate papillae (Fig. 7A), fungiform papillae (Fig. 7B), mucosal epithelium cells (Fig. 7A and 7B), lymphocytes in submucosal tissues of the lingual tonsil (Fig. 7C), and follicular B lymphocytes (Fig. 7D). Spermatogenic cells within the testis were also found to express the gene (Fig. 7E). Gene expression in kidney appeared uniform rather than specific to certain cells (data not shown). We have reached essentially the same in situ hybridization results using a different RNA probe from nt+137 to nt+317 (exon 1 and 2) (data not shown), providing supportive evidence for the findings obtained in the present study.

In order to confirm that swine B lymphocytes expressed *TAS1R3*, mature B lymphocytes were prepared from peripheral blood cells by a cell-sorter using an anti-CD21 antibody

Fig. 7. Expression of *TAS1R3* in swine tissues. Red and black arrows in **A** indicate tongue circumvallate papillae and mucosal epithelium, respectively; in **B**, they indicate tongue fungiform papillae and mucosal epithelium, respectively; (**C**) lymphocytes in submucosal tissue of lingual tonsil; (**D**) follicular B lymphocytes; and (**E**) spermatogenic cells in testis. (A1–E1) Results of in situ hybridization using RNA anti-sense probe (detection of *TAS1R3* sense message); (A2–E2) results of hybridization using RNA sense probe; and (A3–C3) staining with hematoxylin and eosin.

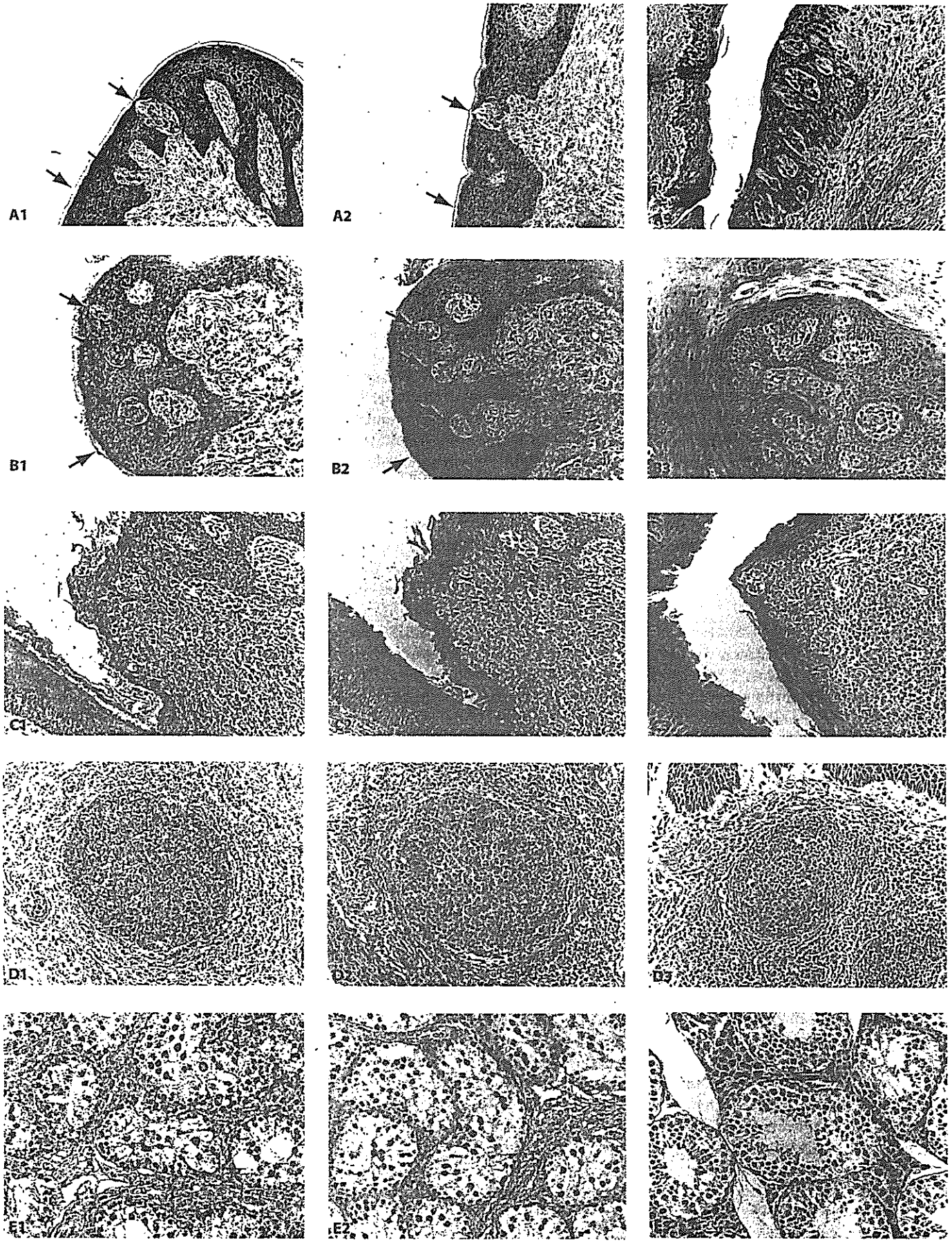
A1
A2
B1
B2
C1
D1
D2
D3
E1
E2

to extract RNA from the lymphocytes. Real-time PCR using that RNA demonstrated the existence of a transcript from *TAS1R3* in B lymphocytes. However, since the amount of RNA prepared from the B lymphocytes was too small to be determined by UV absorbance, the amount of transcript in the B lymphocytes sample could not be directly compared with amounts of transcript in other samples (such as tongue). The DNA fragment amplified from B lymphocytes was cloned and sequenced, and found to be identical to that of *TAS1R3* cDNA. These findings confirmed the expression of *TAS1R3* in B lymphocytes, though the level of that expression could not be determined.

Exploitation of SNPs possibly related to tasting

The association between differences in sweet preference and sequence polymorphisms producing amino-acid substitutions has been previously reported in mouse (Max et al., 2001; Reed et al., 2004). Therefore, genomic DNAs from nine pigs of various breeds (see Materials and methods) were sequenced for the entire *TAS1R3* gene (position: 1055 to 6862 in the sequence with Accession No. AB162126), and the *TAS1R3* genomic sequences were compared. Eight SNPs in exons and five SNPs in introns were identified (described in the annotation of the sequence with Accession No. AB162126). However, no SNPs found in exons produced amino-acid substitutions (data not shown).

Discussion

TAS1R3 has been shown to be involved in sweet and umami tastes (along with TAS1R2 and TAS1R1) in mouse, and the sequence of the gene has been reported in mouse (Accession No. AL670236.9), rat (Accession No. NW_043877.1), gorilla (Accession No. AF545574), and human (Accession No. NT_077965.1). In the present study, the genomic structure of swine *TAS1R3* was determined, and *TAS1R3* expression was studied in various swine tissues. That gene was shown to reside on SSC6q22→q23, from which three distinct mRNA transcripts were generated: a 3,752-bp transcript derived from six exons was found in tongue, whereas in testis a 3,704-bp transcript from six exons, and a 3,630-bp transcript from seven exons were found. The 6-exons/5-introns structure was similar to those observed in human and mouse, but the 7-exons/6-introns structure of *TAS1R3* was first observed in swine. The expression pattern of the *TAS1R3* gene in tongue, testis, heart, lung, and liver was similar to that observed in mouse (Max et al., 2001). Additionally, a high expression with a level similar to that in testis was observed in kidney, a finding which had not previously been reported. In hybridization in situ, *TAS1R3* expression was detected in the tongue circumvallate papillae, fungiform papillae, mucosal epithelium, follicular B lymphocytes, lymphocytes in submucosal tissues of the lingual tonsil, and spermatogenic cells. In kidney, the expression appeared to be uniformly consistent rather than confined to specific cells. The expression of *TAS1R3* in B lymphocytes was further confirmed by real-time PCR using peripheral mature B lymphocytes, and by sequencing of the real-time PCR product.

Since the genomic structure, nucleotide sequence of cDNA, and amino-acid sequences of TAS1R3 are similar in swine, human and mouse, we hypothesized that functional transcription factor binding sites commonly exist in the three species. Based on this hypothesis, sequences upstream of the translation start site were compared to reveal an SRY binding site located 89 bp upstream of the translation start site as the one and only common site in the species. Hence, the SRY binding site is considered to serve as a functional binding site for the *TAS1R3* gene. However, in swine, two types of the exon/intron structures were involved in the generation of transcripts from *TAS1R3*, suggesting that another functional transcription factor binding site should exist. Genes such as the human collagen gene have previously been demonstrated to have functional transcription factor binding sites in their introns (Bornstein et al., 1987; Schultz et al., 1991). When the intron sequences of the three species were compared to identify common transcription factors, it was demonstrated that the Sp1 binding site was identified as a common site in swine and human intron 2. Therefore, it is possible that Sp1 would be another element in differential gene expression.

TAS1R3 expression was detected in the tongue circumvallate papillae, fungiform papillae, mucosal epithelium, follicular B lymphocytes, lymphocytes in submucosal tissues of the lingual tonsil, spermatogenic cells, kidney and peripheral mature B lymphocytes by both or either of real-time PCR and in situ hybridization. The expressions in circumvallate papillae and fungiform papillae were reported in mouse (Kitagawa et al., 2001; Max et al., 2001). However, expressions in tongue mucosal epithelium, kidney, and B lymphocytes have not been previously reported. In taste papillae, complexes of TAS1R1 and TAS1R3, and of TAS1R2 and TAS1R3 serve as the receptors for umami and sweet, respectively (Nelson et al., 2001, 2002). However, since no tasting function is considered to exist in tissues or cells other than the taste receptor cells, and since the types of cells expressing *TAS1R3* gene are different, it is possible that TAS1R3 is involved in different signal transductions in those cells via collaboration with proteins other than TAS1R1 and TAS1R2. In order to provide clues to infer the functions of *TAS1R3* in those cells, expressions of *TAS1R1* and *TAS1R2* should be examined specifically in those cells, while *TAS1R3* expression should be investigated throughout the differentiation processes of those cells.

Acknowledgements

The authors wish to thank Drs. Martine Yerle (INRA, France), Lawrence B. Schook (UIUC, USA), and Craig W. Beattie (UNR, USA) for supplying the IMpRH panel DNA. The authors also wish to thank Dr. Sue Galloway (AgResearch, New Zealand) for critical reading of our manuscript and suggestions in preparation of the manuscript.

References

Adler E, Hoon MA, Mueller KL, Chandrashekar J, Ryba NJ, Zuker CS: A novel family of mammalian taste receptors. Cell 100:693–702 (2000).

Awata T, Yamakuchi H, Kumagai M, Yasue H: Assignment of the tenascin gene *(HXB)* to swine chromosome 1q21.1→q21.3 by fluorescence in situ hybridization. Cytogenet Cell Genet 69: 33–34 (1995).

Bernhardt SJ, Naim M, Zehavi U, Lindemann B: Changes in IP3 and cytosolic Ca^{2+} in response to sugars and non-sugar sweeteners in transduction of sweet taste in the rat. J Physiol 490: 325–336 (1996).

Bornstein P, McKay J, Morishima JK, Devarayalu S, Gelinas RE: Regulatory elements in the first intron contribute to transcriptional control of the human alpha 1(I) collagen gene. Proc Natl Acad Sci USA 84:8869–8873 (1987).

Cummings TA, Daniels C, Kinnamon SC: Sweet taste transduction in hamster: sweeteners and cyclic nucleotides depolarize taste cells by reducing a K^+ current. J Neurophysiol 75:1256–1263 (1996).

Gilbertson TA, Avenet P, Kinnamon SC, Roper SD: Proton currents through amiloride-sensitive Na channels in hamster taste cells. Role in acid transduction. J Gen Physiol 100:803–824 (1992).

Gilbertson TA, Damak S, Margolskee RF: The molecular physiology of taste transduction. Curr Opin Neurobiol 10:519–527 (2000).

Kitagawa M, Kusakabe Y, Miura H, Ninomiya Y, Hino A: Molecular genetic identification of a candidate receptor gene for sweet taste. Biochem Biophys Res Commun 283:236–242 (2001).

Kiuchi S, Inage Y, Hiraiwa H, Uenishi H, Yasue H: Assignment of 280 swine genomic inserts including 31 microsatellites from BAC clones to the swine RH map (IMpRH map). Mamm Genome 13:80–88 (2002).

Kretz O, Barbry P, Bock R, Lindemann B: Differential expression of RNA and protein of the three pore-forming subunits of the amiloride-sensitive epithelial sodium channel in taste buds of the rat. J Histochem Cytochem 47:51–64 (1999).

Li X, Staszewski L, Xu H, Durick K, Zoller M, Adler E: Human receptors for sweet and umami taste. Proc Natl Acad Sci USA 99:4692–4696 (2002).

Lin W, Burks CA, Hansen DR, Kinnamon SC, Gilbertson TA: Taste receptor cells express pH-sensitive leak K^+ channels. J Neurophysiol 92: 2909–2919 (2004).

Lindemann B: Receptors and transduction in taste. Nature 413:219–225 (2001).

Max M, Shanker YG, Huang L, Rong M, Liu Z, Campagne F, Weinstein H, Damak S, Margolskee RF: *Tas1r3*, encoding a new candidate taste receptor, is allelic to the sweet responsiveness locus *Sac*. Nat Genet 28:58–63 (2001).

Mikawa S, Akita T, Hisamatsu N, Inage Y, Ito Y, Kobayashi E, Kusumoto H, Matsumoto T, et al: A linkage map of 243 DNA markers in an intercross of Gottingen miniature and Meishan pigs. Anim Genet 30:407–417 (1999).

Milan D, Hawken R, Cabau C, Leroux S, Genet C, Lahbib Y, Tosser G, Robic A, et al: IMpRH server: an RH mapping server available on the Web. Bioinformatics 16:558–559 (2000).

Nelson G, Hoon MA, Chandrashekar J, Zhang Y, Ryba NJ, Zuker CS: Mammalian sweet taste receptors. Cell 106:381–390 (2001).

Nelson G, Chandrashekar J, Hoon MA, Feng L, Zhao G, Ryba NJ, Zuker CS: An amino-acid taste receptor. Nature 416:199–202 (2002).

Ohtsuki T, Furuya S, Yamada T, Nomura S, Hata J, Yabe Y, Hosoda Y: Gene expression of noncollagenous bone matrix proteins in the limb joints and intervertebral disks of the *twy* mouse. Calcif Tissue Int 63:67–172 (1998).

Reed DR, Li S, Li X, Huang L, Tordoff MG, Starling-Roney R, Taniguchi K, West DB, et al: Polymorphisms in the taste receptor gene (*Tas1r3*) region are associated with saccharin preference in 30 mouse strains. J Neurosci 24:938–946 (2004).

Schultz JR, Tansey T, Gremke L, Storti RV: A muscle-specific intron enhancer required for rescue of indirect flight muscle and jump muscle function regulates *Drosophila* tropomyosin I gene expression. Mol Cell Biol 11:1901–1911 (1991).

Suzuki K, Asakawa S, Iida M, Shimanuki S, Fujishima N, Hiraiwa H, Murakami Y, Shimizu N, Yasue H: Construction and evaluation of a porcine bacterial artificial chromosome library. Anim Genet 31:8–12 (2000).

Suzuki Y, Sugano S: Construction of a full-length enriched and a 5′-end enriched cDNA library using the oligo-capping method. Methods Mol Biol 221:73–91 (2003).

Tumbelson ME, Schook LB: Advances in swine in biomedical research, in Tumbelson ME, Schook LB (eds): Advances in Swine in Biomedical Research, pp 1–4 (Plenum Press, New York 1996).

Yasue H, Ishibashi M: The oncogenicity of avian adenoviruses. III. In situ DNA hybridization of tumor line cells localized a large number of a virocellular sequence in few chromosomes. Virology 116:99–115 (1982).

Yerle M, Pinton P, Robic A, Alfonso A, Palvadeau Y, Delcros C, Hawken R, Alexander L, et al: Construction of a whole-genome radiation hybrid panel for high-resolution gene mapping in pigs. Cytogenet Cell Genet 82:182–188 (1998).

Zhao GQ, Zhang Y, Hoon MA, Chandrashekar J, Erlenbach I, Ryba NJ, Zuker CS: The receptors for mammalian sweet and umami taste. Cell 115:255–266 (2003).

Pediatr Blood Cancer 2007;48:230–232

BRIEF REPORT
Development of Diffuse Large B Cell Lymphoma During the Maintenance Therapy for B-Lineage Acute Lymphoblastic Leukemia

Itaru Kato, MD,[1]* Atsushi Manabe, MD,[1] Chiaki Aoyama, MD,[1] Takahiro Kamiya, MD,[1] Tsuyoshi Morimoto, MD,[1] Hiroshi Matsufuji, MD,[2] Koyu Suzuki, MD,[3] Yoshiro Kitagawa, MD,[4] Toshinori Hori, MD,[4] Masahito Tsurusawa, MD,[4] Nobutaka Kiyokawa, MD,[5] Junichiro Fujimoto, MD,[5] and Ryota Hosoya, MD[1]

Non-Hodgkin lymphoma (NHL) is a very rare complication of acute lymphoblastic leukemia (ALL). A Japanese boy presented with B-lineage ALL at the age of 2.5. He was treated with chemotherapy for standard-risk ALL. While he was receiving maintenance treatment 2 years and 9 months after the diagnosis of ALL, diffuse large B cell lymphoma (DLBL) was diagnosed from a biopsy of an abdominal mass. DLBL was treated by surgical resection followed by chemotherapy for 6 months. The patient has been free from the recurrence of ALL or DLBL for 16 months after the development of DLBL. Pediatr Blood Cancer 2007;48:230–232. © 2006 Wiley-Liss, Inc.

Key words: B-lineage acute lymphoblastic leukemia; diffuse large B cell lymphoma; intussusception

INTRODUCTION

Although the survival rate for children with cancer improved dramatically, the development of secondary malignancies is a serious complication. The incidence of secondary non-Hodgkins lymphoma (NHL) was reported to be only 0.08%, and there were only five cases presenting with large cell lymphoma occurring after the treatment for acute lymphoblastic leukemia (ALL). We describe such a case and discuss the pathophysiology of the disease.

CASE REPORT

A Japanese male presented with a 9-day history of fever. Physical examination revealed hepatomegaly palpated 2 cm below the costal margin. The white blood cell count was 14,000/μl with 21% of lymphoblasts, hemoglobin was 11.0 g/dl, platelet count was 162,000/μl, and lactate dehydrogenase (LDH) was 4,984 IU/L. The bone marrow was normocellular with 71.0% lymphoblasts with L1 morphology. Immunophenotyping of the bone marrow lymphoblasts was positive for CD10, CD19, and HLA-DR, and negative for CD3 and CD20. Karyotype was 46XY, t(2; 6)(q31; p23) in 20 metaphases tested. A diagnosis of B-lineage ALL was made.

The patient was treated according to the protocol of the Tokyo Children's Cancer Study Group (TCCSG) L99-15 standard risk regimen. Induction was with prednisolone, vincristine, therarubicin, and L-asparaginase. Prophylactic central nervous system therapy consisted of intrathecal methotrexate, hydrocortisone, and cytarabine. The disease responded promptly and a complete remission was achieved. The following treatment was identical to that in the previous protocol (L95-14), which was described by Igarashi et al. [1]. Epipodophyllotoxins were not used in this protocol. Maintenance therapy consisted of oral 6-mercaptopurine and methotrexate and began 12 months after the diagnosis.

The patient remained asymptomatic and in complete remission although the karyotypic abnormality remained unchanged.

Two years and 9 months after the diagnosis of ALL, during the maintenance therapy, the patient developed abdominal pain and intussusception, requiring emergency laparotomy. The proximal portion of the intussusception was a small bowel mass measuring 2.8 × 1.8 × 0.8 cm. Several regional lymph nodes were enlarged. Evaluation of tumor cells by immunofluorescence showed that the blasts were positive for CD10, CD20, and CD79a, and negative for CD3 and TdT. Following morphological, cytochemical, and immunological evaluation, a diagnosis of DLBL, centroblastic variant was made (Fig. 1). A bone marrow aspirate and biopsy specimens were normal. The cerebrospinal fluid contained 1 cell/μl without lymphoblasts. Rearrangements of *Ig* genes of the bone marrow smear at the diagnosis of ALL and the biopsy specimens of DLBL were not identical.

A ^{67}Ga total body scan revealed abnormal accumulation in the areas of the liver and the upper abdomen. He was treated according to the TCCSG NHL B01-05 Group C protocol, which contained VP-16, prednisolone, cyclophosphamide, methotrexate, epirubucin, vincristine, cytarabine,

[1]Department of Pediatrics, St. Luke's International Hospital, 9-1, Akashi-cho, Chuo-ku, Tokyo 104-8560, Japan; [2]Department of Pediatric Surgery, St. Luke's International Hospital, 9-1, Akashi-cho, Chuo-ku, Tokyo 104-8560, Japan; [3]Department of Pathology, St. Luke's International Hospital, 9-1, Akashi-cho, Chuo-ku, Tokyo 104-8560, Japan; [4]Department of Pediatrics, Aichi Medical University, 9-1, Akashi-cho, Chuo-ku, Tokyo 104-8560, Japan; [5]Department of Developmental Biology and Pathology, National Research Institute for Child Health and Development, 9-1, Akashi-cho, Chuo-ku, Tokyo 104-8560, Japan

*Correspondence to: Dr. Itaru Kato, Department of Pediatrics, Kyoto University, 54 Kawahara-cho, shogoin, Sakyo-ku, Kyoto 606-8501, Japan.

Received 5 May 2005; Accepted 24 April 2006

DOI 10.1002/pbc.20909